THE UNIVERSITY of EDINBURGH

Edinburgh Research Explorer

A synthesis of approaches for modelling coupled thermal–hydraulic–mechanical–chemical processes in a single novaculite fracture experiment

Citation for published version:
Bond, AE, Bruský, I, Cao, T, Chittenden, N, Fedors, R, Feng, X, Gwo, J, Kolditz, O, Lang, P, Mcdermott, C, Neretnieks, I, Pan, P, Šembera, J, Shao, H, Watanabe, N, Yasuhara, H & Zheng, H 2017, 'A synthesis of approaches for modelling coupled thermal–hydraulic–mechanical–chemical processes in a single novaculite fracture experiment', *Environmental Earth Sciences*, vol. 76, no. 1. https://doi.org/10.1007/s12665-016-6326-6

Digital Object Identifier (DOI):
10.1007/s12665-016-6326-6

Link:
Link to publication record in Edinburgh Research Explorer

Document Version:
Peer reviewed version

Published In:
Environmental Earth Sciences

Publisher Rights Statement:
© Springer-Verlag Berlin Heidelberg 2016

General rights
Copyright for the publications made accessible via the Edinburgh Research Explorer is retained by the author(s) and / or other copyright owners and it is a condition of accessing these publications that users recognise and abide by the legal requirements associated with these rights.

Take down policy
The University of Edinburgh has made every reasonable effort to ensure that Edinburgh Research Explorer content complies with UK legislation. If you believe that the public display of this file breaches copyright please contact openaccess@ed.ac.uk providing details, and we will remove access to the work immediately and investigate your claim.

OPEN ACCESS

Download date: 07. May. 2023

A synthesis of approaches for modelling coupled thermal–hydraulic–mechanical–chemical processes in a single novaculite fracture experiment

Alexander E. Bond, [1,*]

Phone +44(0)1925 885951
Email alexbond@quintessa.org

Ivan Bruský, [2]

Tianqing Cao, [3]

Neil Chittenden, [1]

Randall Fedors, [3]

Xia-Ting Feng, [4]

Jin-Ping Gwo, [3]

Olaf Kolditz, [8]

Philipp Lang, [5]

Christopher McDermott, [6]

Ivars Neretnieks, [7]

Peng-Zhi Pan, [4,*]

Email pzpan@whrsm.ac.cn

Jan Šembera, [2]

Hua Shao, [9]

Nori Watanabe, [8]

Hide Yasuhara, [10]

Hong Zheng, [4]

[1] Quintessa Ltd, Henley-on-Thames, UK

[2] Technical University of Liberec, Liberec, Czech Republic

[3] U.S. Nuclear Regulatory Commission, North Bethesda, MD, USA

[4] Institute of Rock and Soil Mechanics, Chinese Academy of Sciences, Wuhan, China

[5] Imperial College, London, UK

[6] School of Geosciences, University of Edinburgh, Edinburgh, UK

[7] Department of Chemical Engineering, Royal Institute of Technology, Stockholm, Sweden

[8] Department Environmental Informatics, Helmholtz Centre for Environmental Research – UFZ, Leipzig, Germany

[9] Federal Institute for Geosciences and Natural Resources (BGR), Hannover, Germany

[10] Ehime University, Matsuyama, Japan

Abstract

The geological formation immediately surrounding a nuclear waste disposal facility has the potential to undergo a complex set of physical and chemical processes starting from construction and continuing many years after closure. The DECOVALEX project (DEvelopment of COupled models and their VALidation against EXperiments) was established and maintained by a variety of waste management organisations, regulators and research organisations to help improve capabilities in experimental interpretation, numerical modelling and blind prediction of complex coupled systems. In the present round of DECOVALEX (D-2015), one component of Task C1 has considered the detailed experimental work of Yasuhara et al. (Earth Planet Sci Lett 244:186–200, 2006), wherein a single artificial fracture in novaculite (micro- or crypto-crystalline quartz) is subject to variable fluid flows, mechanical confining pressure and different applied temperatures. This paper presents a synthesis of the completed work of six separate research teams. A range of approaches are presented including 2D and 3D high-resolution coupled thermo–hydro–mechanical–chemical models. The results of the work show that while good, physically plausible representations of the experiment can be obtained using a

range of approaches, there is considerable uncertainty in the relative importance of the various processes, and that the parameterisation of these processes can be closely linked to the interpretation of the fracture surface topography at different spatial scales.

AQ1

AQ2

AQ3

This article is part of a Topical Collection in Environmental Earth Sciences on 'DECOVALEX 2015', guest-edited by Jens T. Birkholzer, Alexander E. Bond, John A. Hudson, Lanru Jing, Hua Shao and Olaf Kolditz.

Disclaimer The views expressed herein do not necessarily reflect the views or regulatory positions of the US Nuclear Regulatory Commission (USNRC) and do not constitute a final judgment or determination of the matters addressed or of the acceptability of any licensing action that may be under consideration at the USNRC. Also, no responsibility is assumed by the authors for any damage to property or persons as a result of operation or use of this publication and/or the information contained herein.

Introduction

Understanding the likely behaviour of fractured rock under variable chemical (C), hydraulic (H), thermal (T) and mechanical (M) conditions in close proximity to a radioactive waste disposal facility is of interest for safety cases supporting a number of disposal concepts. The evolution of fracture permeability can have important impacts for the resaturation of the facility and long-term transport of any radionuclides that escape the immediate area of disposal.

While such systems have been looked at before both within the DECOVALEX project and elsewhere, attempts to model a fully coupled THMC system on a single fracture have been limited. Examples where THMC analysis in fracture rock has been addressed include Yasuhara and Elsworth (2006), Taron et al. (2009) and Zhang et al. (2012), but with the exception of Yasuhara and Elsworth (2006); the emphasis has been largely on theoretical studies, with no direct comparison against well-constrained small-scale experimental data. There is, however, a large body of knowledge concerning THM behaviour with non-reactive transport in fractures (e.g. Berkowitz 2002; Neuman 2005) and a wide range of work examining chemical interactions in fractured systems (e.g. Watson et al. 2016), but modelling efforts incorporating THMC processes for single fractures are rare.

AQ4

The objective of this task (Task C1: one of the five tasks in the current round of DECOVALEX; please see www.decovalex.org for more information on DECOVALEX including numerous examples of this type of collaborative research) is to use the experimental data of Yasuhara et al. (2006, 2011) to model evolving single fractures incorporating coupled THMC effects for novaculite (quartzite) and granite fractures. This work is not focussed on blind prediction, but rather it is focussed on building experience and understanding of the physical processes in operation in such single fractures on the basis of experimental data and understanding of how to represent such processes through numerical and/or semi-analytical models.

This paper focusses only on the novaculite experiment of Yasuhara et al. (2006); the granite experiments are different in many regards and are described elsewhere (Bond et al. 2016); however, this work formed a basis upon which the granite experiments were examined. The task has had significant technical contributions from six teams (abbreviations, where used, are shown in bold), as well as input from Neretnieks (2014) and Sandia National Laboratory:

- **BGR/UFZ**—Germany—Federal Institute for Geosciences and Natural Resources and the Helmholtz Centre for Environmental Research.
- **CAS**—China—Institute of Rock and Soil Mechanics, Chinese Academy of Sciences
- **NDA**—UK—UK Nuclear Decommissioning Authority, Radioactive Waste Management (RWM)
    - **ICL**—Imperial College London
    - **Q** and **UoE**—Quintessa Ltd and the University of Edinburgh
- **NRC**—USA—US Nuclear Regulatory Commission
- **TUL**—Czech Republic—Technical University of Liberec.

It is not the intention of this paper to provide an exhaustive description of the individual contributions from each team, but rather to give a technical overview and synthesis of key conclusions and results. Citations are given to the more detailed contributions from each team via the publication list on the DECOVALEX Web site http://www.decovalex.org/resources.html#special-issues. The various codes and approaches used by the teams are summarised in "Appendix".

Experimental data

The novaculite experiment (Yasuhara et al. 2006) considers the THMC evolution of an artificially fractured sample of Arkansas novaculite (50 mm diameter × 89.5 mm length; micro- or crypto-crystalline quartz with only minor amorphous quartz component), containing only a single induced fracture. The fracture was subject to the following conditions and measurements:

1. Pre-experiment fracture surface profiling using a laser profilometer technique to establish a fracture surface topography.
2. Hydraulic isolation and variable prescribed flow rates of deionised water across the fracture.
3. Mechanical confinement through the application of a confining pressure (1.72 MPa, resulting in an effective stress of ca 1.4 MPa).
4. Heating of the whole sample to different temperatures with time.
5. Measurement of the chemical composition of the outflow and inflow; dissolved Si (ppm) and pH.
6. Measurement of differential pressures across the sample.
7. Post-experiment measurement of the fracture apertures using Wood's metal injection.

The evolution of the pressure difference for a given flow rate gives an indication of the effective hydraulic aperture across the specimen. The general experimental design is shown in Fig. 1. An illustration of the fracture surface topography (not aperture) is shown in Fig. 2.

Fig. 1

Experimental arrangements from the novaculite experiment (modified from Yasuhara et al. 2006); *arrow* shows the designated positive flow direction (Figs. 2, 3)

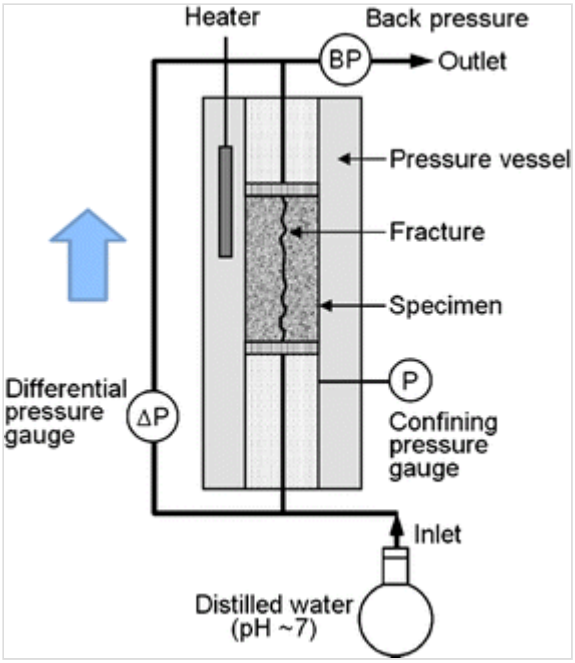

Fig. 2

Topography of one side of the novaculite fracture prior to the experiment; positive flow direction is shown using the *arrows*. Units are in mm from reference elevation, with no vertical exaggeration. Data are as presented in Yasuhara et al. (2006)

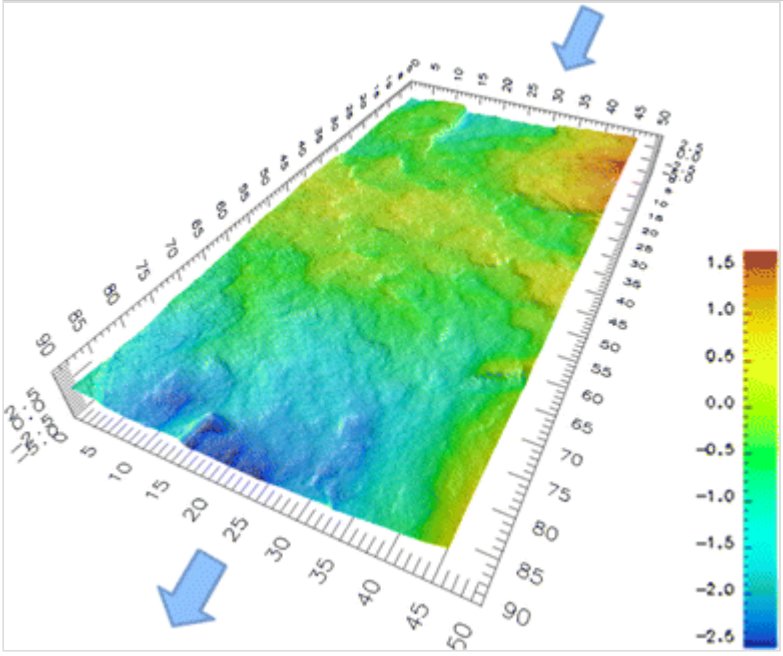

AQ5

The differential pressures are normalised so that pressure differentials can be more easily compared (from Yasuhara et al. 2006):

$$\Delta p_{\mathrm{n}} = \Delta p_{\mathrm{r}} \frac{Q_0}{Q} \frac{\mu_0}{\mu} \quad (1)$$

where Δp_n and Δp_r are the normalised and recorded differential pressures, respectively. Q and μ are flow rate and dynamic viscosity of fluid, and the subscript 0 denotes initial conditions.

The experimental regime over the 3150-h experiment is shown in Fig. 3. The sample is subject to reducing flow rates during the first half of the experiment, broadly reflecting the reduction in fracture transmissivity, but also including a period of flow reversal (isothermal period—water flow was induced in the opposite direction to that shown in Fig. 1). This was then followed by a stepwise increase in temperature peaking at 120 °C (non-isothermal period) and a small increase in flow rate. One key period of the experiment was between 858 and 930 h where complete fluid pressurisation of the sample was lost; this is referred to as the 'shutdown period'.

Fig. 3

Changes applied to water flow rate and temperature throughout the experiment for the novaculite case

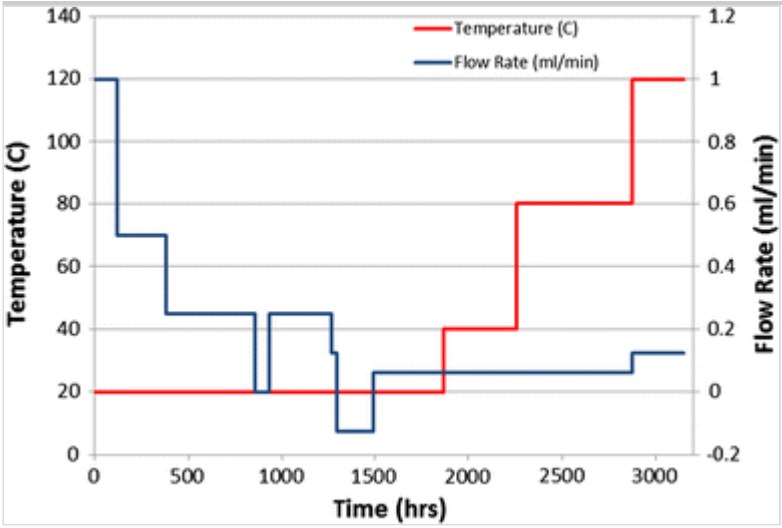

The experimental data show a progressive increase in normalised differential pressure (and hence a corresponding decrease in implied hydraulic aperture—Fig. 4) which is largely insensitive to the flow rate, with a much more complex evolution once the flow reverses and temperature effects come into play. Stepwise changes in hydraulic aperture and rate of change of aperture can be often seen, corresponding to changes in flow rate, and most notably after the shutdown period. The silicon (Si) concentration (Fig. 5) shows a much simpler evolution with a relatively constant outflow concentration observed during the isothermal period, with major changes in concentration only being observed as the temperature changes. The pH results are not discussed here as the significant unstructured variation in both input and output pH was considered unreliable due to CO_2 contamination.

Fig. 4

Measured normalised differential pressure and implied hydraulic aperture with shutdown period highlighted (graphical presentation modified from Yasuhara et al. 2006)

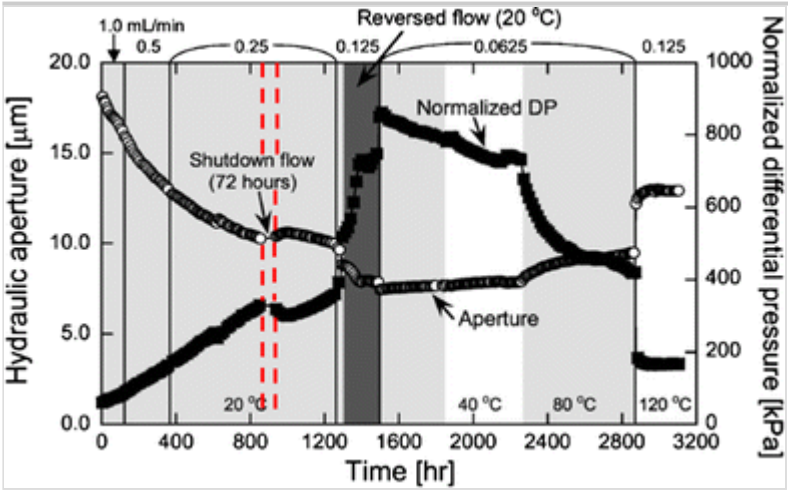

Fig. 5

Measured outflow Si concentration (ppm) with the flow reversal highlighted (graphical presentation modified from Yasuhara et al. 2006)

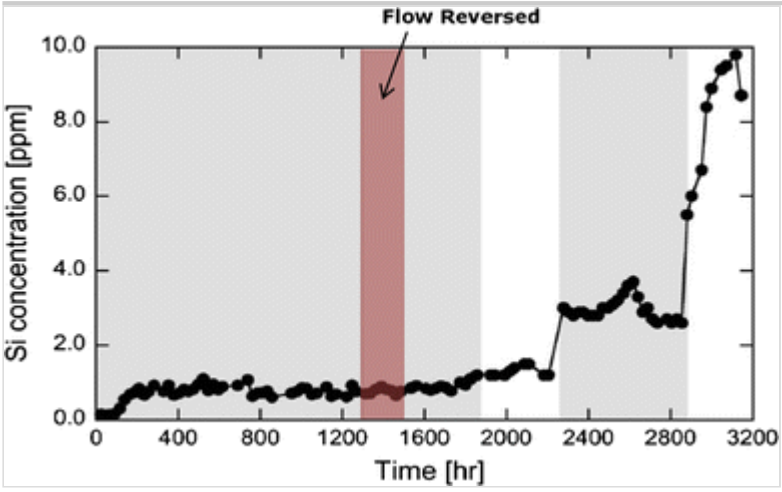

Research team organisation

Task C1 within DECOVALEX-2015 was organised into a series of project 'Steps' (one approximately every 6 months), each of which increases the complexity or the range of experimental complexity being considered by teams. At the end of each step, the work of the teams (see "Introduction" section) was compared and analysed through an open forum—a form of internal peer review.

An important element of the joint work, in addition to attempting to reproduce the experimental results, was 'free' and 'prescribed' geochemical benchmarking of a

highly simplistic synthetic system considering the dissolution of quartz. This allowed the teams to understand the range of responses likely through the use of different geochemical databases and to ensure that the same geochemical response could be achieved if the same input data were specified. The work illustrated that complete parity could be obtained under prescribed conditions, but that differences in quartz solubility and solubility rates of at least a factor of two could be obtained depending on the data source adopted from the literature (Rimstidt 1997; Johnson et al. 1992; Dove and Crerar 1990; Tester et al. 1994; Palandri and Kharaka 2004). More details of the benchmarking and the modelling results in general are given in Bond (2016).

From this approach, a measure of confidence could be built that the results of the teams were genuinely comparable and hence insight could be gained from the range of analyses.

Physicochemical models

It was recognised by all the teams that there are collections of processes that induce the net effects seen in the experimental data. Teams considered the following three net behaviours, albeit in different combinations and relative magnitudes with time:

- Removal of quartz from the fracture surface that gives rise to opening of the fracture (chemical-dominated opening).
- Removal of quartz from the fracture surface that gives rise to closing of the fracture (chemical-dominated closure).
- Closure of the fracture with little or no direct discharge of silicon to the water (mechanical-dominated closure).

Following the initial work of Yasuhara et al. (2006) and Yasuhara and Elsworth (2008), two general sets of physicochemical models were utilised by the teams. The first model considered pressure solution as the dominant mechanism by which both aperture closure and elevated concentrations of Si in the effluent could be obtained, along with conventional free face aqueous dissolution. Following transition state theory (Eyring 1935), the general form of the pressure solution function is as follows:

$$\frac{\mathrm{d}m_{\mathrm{ps},i}}{\mathrm{d}t} = k^{+}\alpha A_{\mathrm{ps},i}\exp\left(\frac{\Delta\mu}{RT}\right)\left(1-\frac{C_i}{C_{\mathrm{eq}}^{\sigma}}\right) \quad 2$$

$$\Delta\mu = \frac{\sigma_{\mathrm{a}} - \sigma_{\mathrm{c}}\beta_{\mathrm{c}}^{2}}{\alpha}V_{\mathrm{m},i} \quad 3$$

$$\Delta b_{\mathrm{ps},i} = -\frac{\Delta m_{\mathrm{ps},i} V_{\mathrm{m},i}}{\alpha A_i} \quad 4$$

where $m_{\mathrm{ps},i}$ is the change in mass of species i (quartz in this case) due to pressure solution, k^+ is the pressure dissolution rate constant (mol/m^2/s), C_i is the concentration of species i in the fluid (ppm), C_{eq}^{σ} is the stress-enhanced solubility of i (ppm), α is an empirical roughness factor (–), $A_{\mathrm{ps},i}$ is the local effective area of species i (m^2) for pressure solution, σ_{a} is the effective stress over the area of contact (Pa), σ_{c} is the critical stress (Pa), β_{c} is the 'burial constant' (–), Δb_i is the incremental change in aperture due to the change in mass of species i, $V_{\mathrm{m},i}$ is the molar volume of species i (m^3/mol), R is the gas constant (J/mol/K), and T is the temperature (K). Aqueous dissolution/precipitation was modelled using conventional transition state theory:

$$\frac{\mathrm{d}m_{\mathrm{d},i}}{\mathrm{d}t} = kA_{e,i}(S)\left(1 - \frac{Q}{K}\right) \quad 5$$

where $m_{\mathrm{d},i}$ is the change in molar mass of species i (quartz in this case) due to dissolution/precipitation, k is the dissolution rate constant (mol/m^2/s), t is time (s), $A_{e,i}(S)$ is the mineral reactive surface area (m^2), Q is the ion activity product for the solid of interest (dimensionless), and K is the equilibrium constant for mineral dissolution (dimensionless).

It should be noted that all teams, with the exception of BGR/UFZ and consistent with Yasuhara et al. (2006), elected not to place $\frac{\Delta\mu}{RT}$ within an exponential term and exclude the concentration dependence, and hence used a simpler form:

$$\frac{\mathrm{d}m_{\mathrm{ps},i}}{\mathrm{d}t} = k^+ A_{\mathrm{ps},i} \frac{3V_{\mathrm{m}}(\sigma_{\mathrm{a}} - \sigma_{\mathrm{c}})}{RT} \quad 6$$

In addition, most teams added empirical scaling factors to different parts of the above relationship to improve their calibration, but the basic formulation was retained—see "Calibration and model results" section for the discussion on selected parameterisation. The conceptual model for the pressure solution is illustrated schematically in Figs. 6 and 7.

Fig. 6

Schematic illustration of the pressure solution-based mathematical model adopted by the CAS team. A_e is the area associated with fracture porosity, σ_{eff} is the effective stress, and σ_{a} is the contact area stress. More details of the CAS approach are given in Pan et al. (2016)

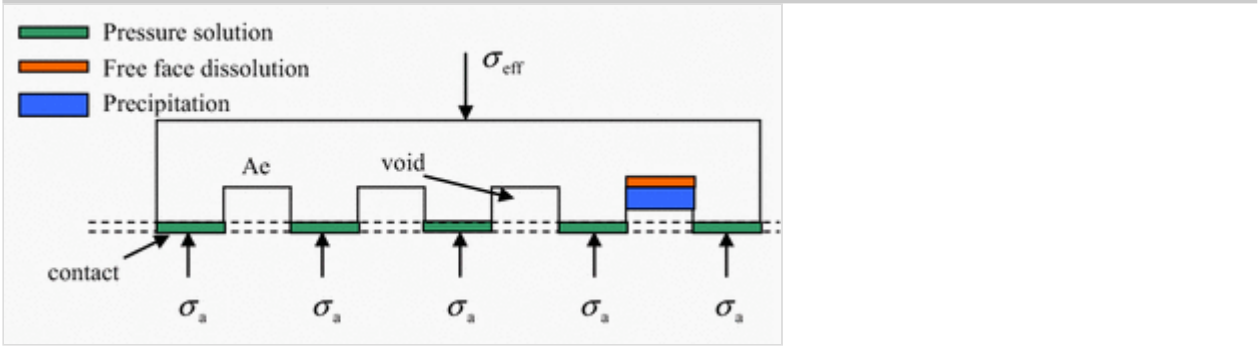

Fig. 7

Conceptual model for the fracture system as adopted by the BGR/UFZ team showing different scales of interest over which key processes may be considered to occur. Note that the CAS schematic conceptual model in Fig. 6 essentially corresponds to the 'macroscopic' scale

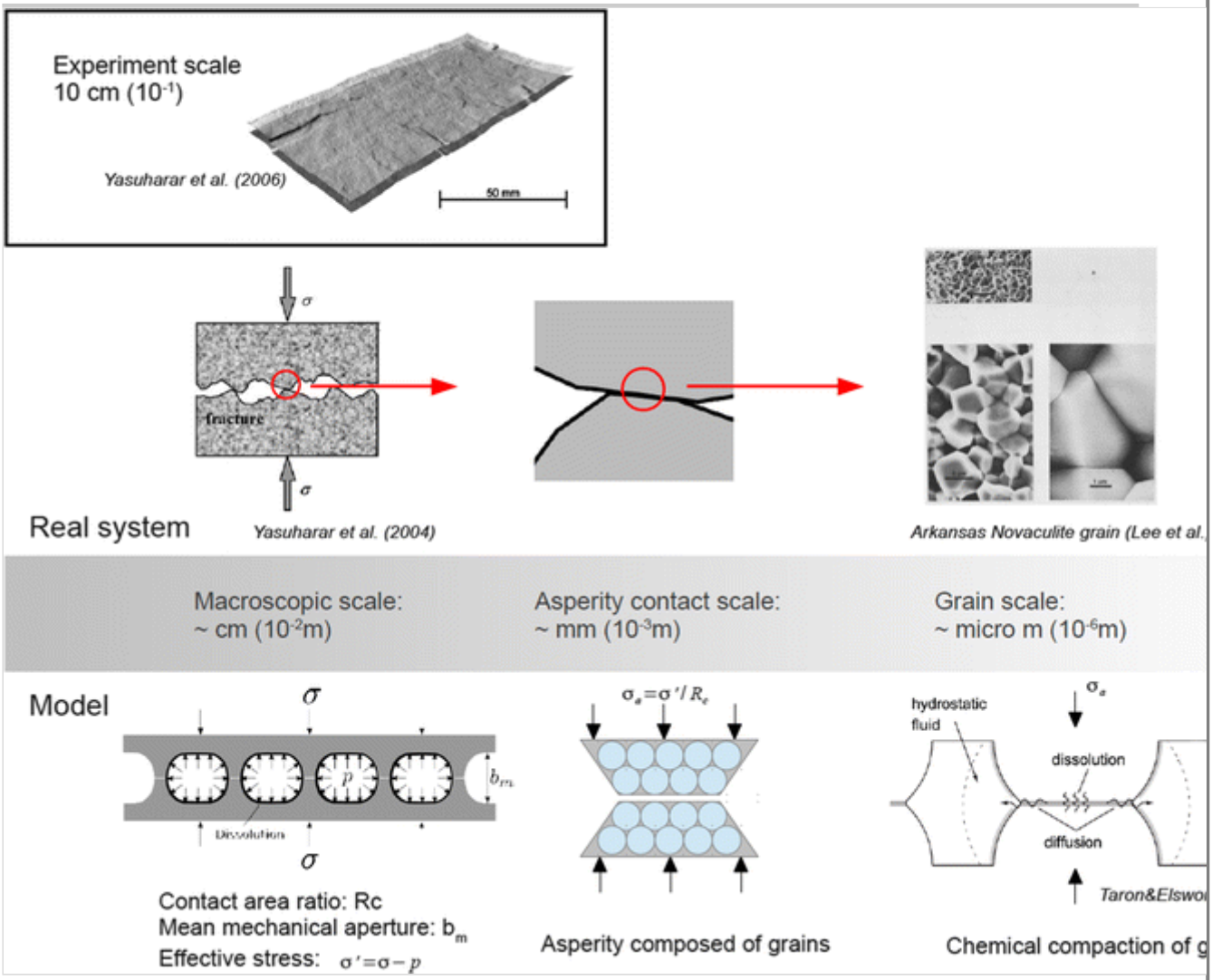

It should be noted that the use of a nonzero critical stress was considered by some teams to be thermodynamically unsound, on the basis that any increase in stress increases the potential for dissolution. Other teams considered that using a nonzero stress was justified by the experimental data and represents a combination

of a complex set of processes that allows a fracture to reach an equilibrium closure state.

The alternative model considered a process of ‘stress corrosion’ where the low concentrations of inflowing water induce micro-mechanical failure of the grains under load giving rise to aperture closure through chemically enhanced mechanical effects (Yasuhara and Elsworth 2008). The process is illustrated schematically in Fig. 8. Such a process model does not give rise to additional silicon in solution directly, but the mechanical failure may be considered to give rise to additional mineral area through which dissolution may occur. The form of stress corrosion model with reference parameterisation adopted by teams is as follows (Yasuhara and Elsworth 2008; Dove 1995)

$$\frac{\mathrm{d}b}{\mathrm{d}t} = -(1 - R_{\mathrm{c}})\, v_{\mathrm{Si\text{-}O}} \tag{7}$$

$$v_{\mathrm{Si-O}} = A_{\mathrm{H_2O}} \exp\left(-\frac{\Delta H_{\mathrm{H_2O}}}{RT}\right) \exp\left(b^{*}_{\mathrm{H_2O}} K_{\mathrm{I}}\right) \left(\theta^{\mathrm{H_2O}}_{\mathrm{Si\text{-}O}}\right) + A_{\mathrm{OH^-}} \exp\left(-\frac{\Delta H_{\mathrm{OH^-}}}{RT}\right) \exp\left(b^{*}_{\mathrm{OH^-}} K_{\mathrm{I}}\right)$$

where $A_{\mathrm{H_2O}}$ and $A_{\mathrm{OH^-}}$ are pre-exponential factors (m/s), $b^{*}_{\mathrm{H_2O}}$, $b^{*}_{\mathrm{OH^-}}$ are constants derived from the geometry of crack tips ($\mathrm{N^{-1}\ m^{3/2}}$), $\theta^{\mathrm{H_2O}}_{\mathrm{Si\text{-}O}}$ and $\theta^{\mathrm{OH^-}}_{\mathrm{Si\text{-}O}}$ are the fractions of $\mathrm{H_2O}$ and the fraction of $\mathrm{OH^-}$ reacting with Si–O, respectively, R_{c} is the local contact ratio, and K_{I} is the stress intensity factor defined as (Atkinson 1987):

$$K_{\mathrm{I}} = \lim_{r=0} \left[\sigma_y (2\pi r)^{\frac{1}{2}}\right] \tag{9}$$

where σ_y is the tensile stress applied at or close to the crack tip (Pa) and r, parallel to the crack growth direction, is the infinitesimal distance from the crack tip (m). A more complete description of the process, parameterisation and the necessary simplifications for the stress corrosion process is given in Yasuhara and Elsworth (2008).

Fig. 8

Schematic illustration of the stress-corrosion-induced micro-cracking (from Yasuhara and Elsworth 2008) showing the conceptualisation at the ‘macroscopic’ scale (to compare with Figs. 6, 7) and the single asperity scale

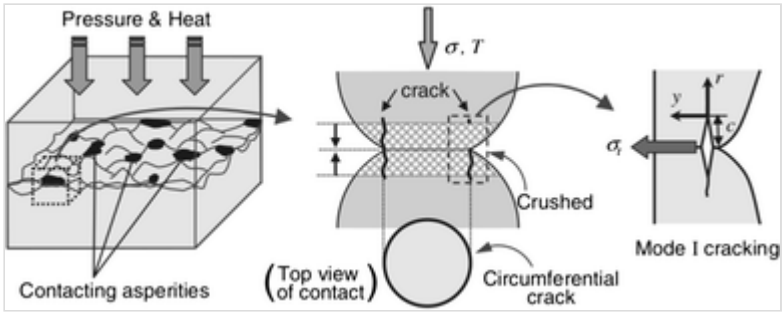

AQ6

In all cases, viscous-dominated ‘Darcy’ flow was adopted by the teams for fluid flow (Fetter 1994) with the ‘cubic law’ relationship between permeability and mechanical aperture. However, BGR/UFZ did find a generally improved calibration by using the Walsh model (Walsh 1981) to relate hydraulic and mechanical apertures:

$$b_{\mathrm{h}}^{3} = \frac{1 - R_{\mathrm{c}}}{1 + R_{\mathrm{c}}} b_{\mathrm{m}}^{3} \qquad 10$$

where R_{c} is the local contact ratio (dimensionless) and b_{h} and b_{m} are the hydraulic and mechanical apertures, respectively (m).

Transport of dissolved species was generally achieved through the conventional advection–dispersion equation (Poon et al. 1992), although some teams neglected the diffusive/dispersive process (e.g. UoE—McDermott et al. 2015).

Modelling approaches

Three different modelling approaches have been attempted by the participating teams:

1. Discretised (2D) models—taking the fracture topography data to locally define a mechanical and hence hydraulic aperture and solve the process models across a 2D representation of the fracture (**BGR/UFZ**, **CAS**, ICL, UoE, **TUL**, Q).

2. Homogenised (0D/1D/2D) models—treating the entire fracture surface as a single entity (all teams, early data only; **NRC**—closure only, **Q**, **CAS**—full time series).

3. Synthetic models—using the fracture topography data to define a statistical description of the fracture aperture distribution at different spatial scales and using this to inform physical models (BGR/UFZ, **ICL**, **UoE**).

Note that some teams attempted multiple approaches during the project, entries in bold indicate the final approach adopted and the results presented. Within these

three general groups, there are various approaches for solving the numerical problem including multi-scale and hybridised analytical and numerical techniques; these will be discussed for each team in turn.

The mechanism adopted by most teams for deriving the detailed grids for ~~D~~discretised models is outlined in Fig. 9. The approach takes the topography of the two sides of the fracture aperture and subtracts one surface from the other on a point-by-point basis with an addition of a constant offset between surfaces to create a net aperture. Where the resulting aperture is zero or negative, contact between the two surfaces is assumed to occur; hence, a relationship between net aperture and contact ratio can be estimated (Fig. 10). The resulting aperture map is then calibrated by the constant offset on the aperture map, such that the experimentally derived bulk fracture transmissivity and/or contact ratio is reproduced by the resulting aperture map. As discussed later, there are several issues with this approach to interpreting the data, some of which can lead to quite different aperture distributions.

Fig. 9

Schematic illustration of the process of deriving grids using the ‘detailed’ approach from ICL (noting that ICL’s final model uses a ‘synthetic’ technique)

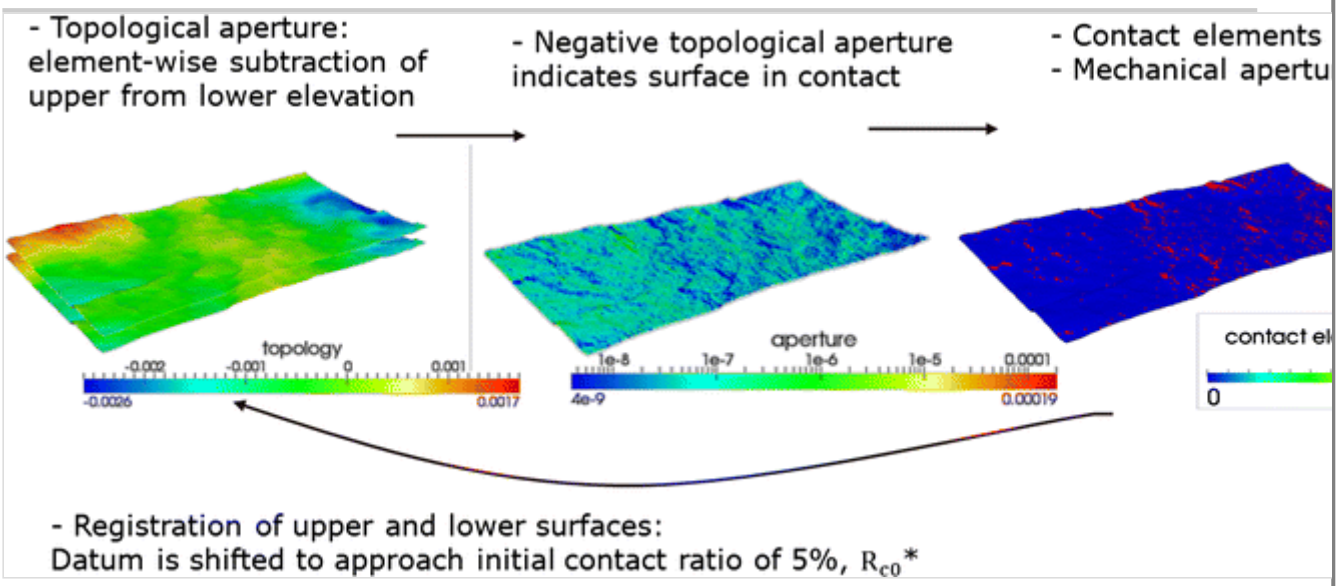

Fig. 10

Aperture versus contact ratio plot (from Yasuhara et al. 2006), where R_{c0} is the initial contact ratio

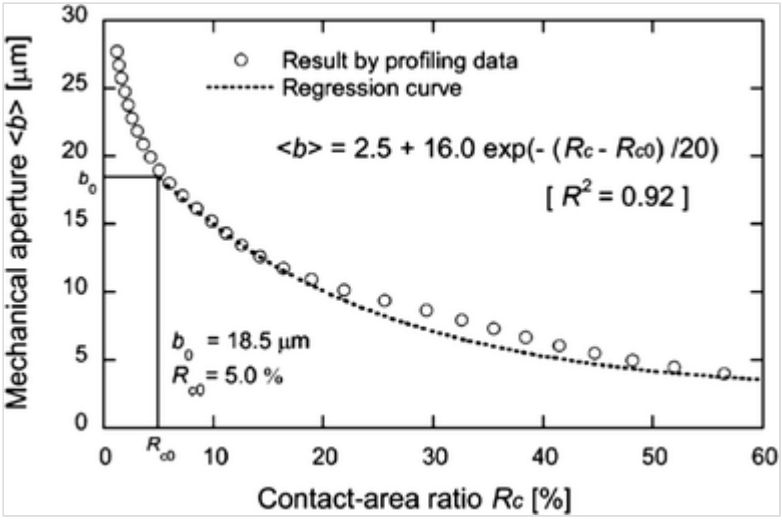

AQ7

Considerable effort was spent by some teams establishing the minimum resolution at which such an approach is valid, bearing in mind that each surface comprises ~1.6 million data points and is therefore not practicable for direct numerical analysis. The UoE team from their finite element analysis found that results were not appreciably different when de-refining the aperture data to a 0.8-mm (from 50 μm) quadrilateral grid. The results of the grid convergence study are discussed in Bond et al. (2015a), and it is noted that a similar exercise was performed by Pan et al. (2016) which gave similar results. This led to a reduction in data points to ~6000 while still representing the main features of the fracture closure. The mechanical closure processes could then be applied on an elemental piecewise basis, with coupling between the closure and the effective permeability of that element, and the redistribution of stress when fracture elements closed sufficiently to be in contact. Flow and transport processes are also adopted on an element basis, calculating water movement assuming viscous-dominated flow and transport of dissolved species using the advection–dispersion relationship. BGR/UFZ, TUL and CAS used this method for their final models.

Coupling was achieved either through fully implicit methods (Q—Chittenden et al. 2016) or stepwise coupling (all other teams), but the choice of numerical method did not appear to significantly impact the results.

In contrast, the homogenised models used the aperture maps to construct a mechanical aperture versus contact ratio correlation (e.g. Fig. 10) and use this relationship in place of a highly discretised fracture surface. Many of the teams independently recalculated the distribution (e.g. Chittenden et al. 2016; McDermott et al. 2015) based on the fracture surface topography data and obtained very similar results to the distribution adopted by Yasuhara et al. (2006) as shown in Fig. 10.

This relationship permits the effective contact ratio to be determined as the aperture changes and hence allows the various areas and contact stresses to be estimated and updated dynamically as the aperture evolves. The homogenised approach can be used both in 0D (single lumped parameter model), but also in a discretised 2D scheme where initial aperture (and hence initial contact ratio) is permitted to vary and simple mechanical coupling is established across the surface to redistribute stresses. As the resolution is increased, such a homogenised method will tend to look more like the discretised approach.

NRC extended the approach given above to explicitly consider multi-scale issues whereby the loss of dissolved Si from a contact point is controlled by diffusion across a boundary layer around the asperity (adopted from Yasuhara et al. 2011). In their case, they assumed:

$$\frac{\mathrm{d}m_{\mathrm{diff},i}}{\mathrm{d}t} = 8\pi D_{b,i}\omega\left(C_{\mathrm{int},i} - C_{\mathrm{pore},i}\right) \quad (11)$$

where D_b is the diffusion coefficient, ω is the thickness of the water film within the asperity contact (assumed to be 4 nm wide), and C_{int} and C_{pore} are the mineral concentrations of species *i* within the water film and open fracture space, respectively. In this model, $\frac{\mathrm{d}m_{\mathrm{diff},i}}{\mathrm{d}t}$ and $\frac{\mathrm{d}m_{\mathrm{ps},i}}{\mathrm{d}t}$ described in Eq. (6) are constrained to be equal.

The synthetic models use the fracture topography data to describe the fracture surface in a statistical sense and then use that information to inform physical models, rather than using the fracture 'aperture' information directly. Three approaches were considered. The first (BGR/UFZ) takes the data at the scale of the profilometer measurement and establishes a variogram that reflects that statistical distribution. Multiple realisations of the surface and the behaviour of that surface can then be compared using the discretised approach. Flow, transport and mechanical effects are then calculated on this 2D discretised grid following the '~~D~~discretised' method but using a synthetic fracture representation.

The second method (ICL) recognises the scale dependence of the fracture surface roughness. Using assumptions of a Gaussian topography height distribution and self-affine organisation, one can decompose the surface roughness using Fourier transformation to associate amplitudes and length scales with the observations. This generates a roughness spectrum or power spectral density (PSD) which in turn is described by a Hurst exponent (Poon et al. 1992; Schmittbuhl et al. 1995) and a surface roughness amplitude.

This statistical representation of the fracture surface is then used to generate a sufficiently large area of the fracture surface to be considered a representative elementary volume (REV)—5 × 5 cm for the ICL novaculite case (Fig. 11)—and uses this to model elastic compression for the whole fracture on a 512 × 512 local grid. It was assumed that an REV was applicable here as the size of the surface is large in comparison with the single fracture, but this assertion was not directly tested but felt to be robust by ICL. More details are available in Lang et al. (2015). The elastic, frictionless contact of two surfaces is reduced to the contact between a rigid composite surface and a planar surface of an elastic body of infinite extent and elastic composite moduli (Brown and Scholz 1985, see Fig. 12).

Fig. 11

REV elastic contact model for the fracture and the corresponding 1D advection–dispersion model (ICL)

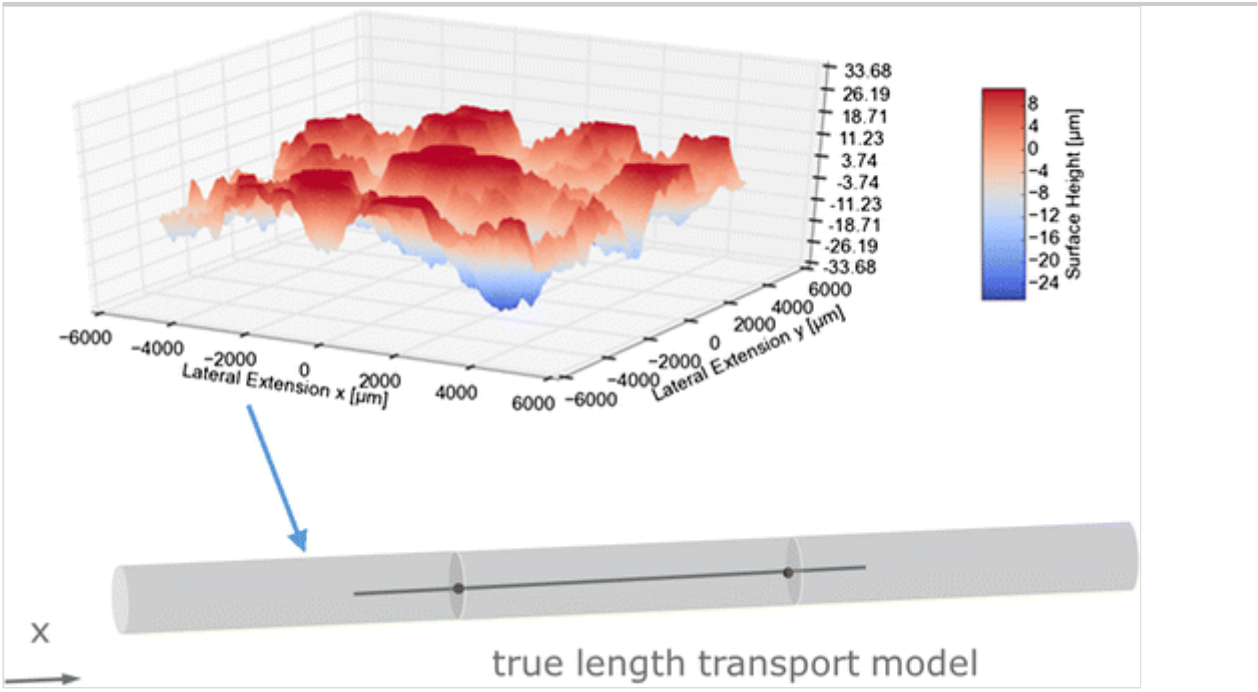

Fig. 12

Part of a cross section of the elastic contact model between the rigid composite surface and the elastic body. Pressure solution over the contacting surface fraction acts to compact the fracture, while free face dissolution simultaneously increases transmissivity by extending existing flow channels. The label R_c marks the current contact ratio, which increases with time. The *shaded area* marks the elastic deflection of the fracture. Note the scaling difference between ordinate and abscissa (ICL)

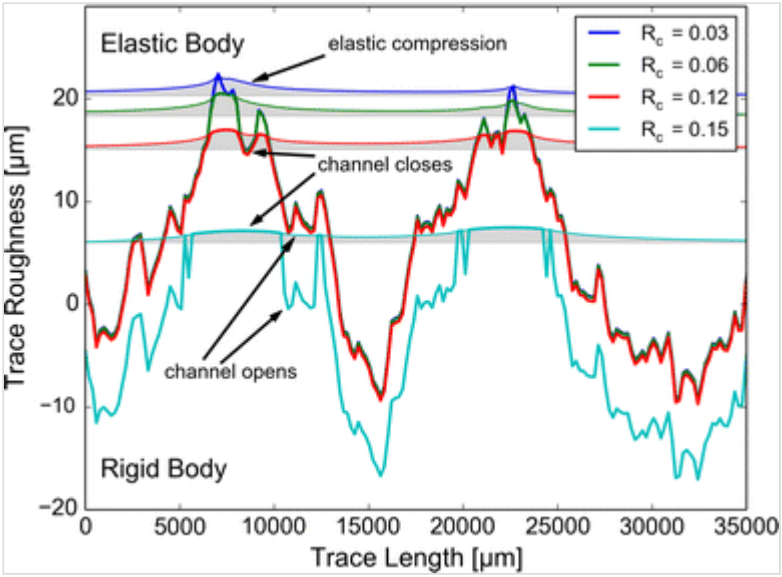

The evolution of this REV is then used to parameterise a 1D advection–dispersion transport (including free face dissolution) model representing the full length of the fracture (Fig. 11). Effective transmissivity is calculated using a numerical solution in 2D of the lubrication equation (Zimmerman et al. 1991) to calculate permeability on the basis of the mechanical aperture field and resulting flow for the REV model (Lang et al. 2015).

The third method (UoE, Q) involved statistical consideration of fracture asperities and generation of fracture aperture surfaces for use in a high-resolution finite element grid. UoE considered that examination of the novaculite surface scan data shows that there are two scales of surface profile roughness: the aperture ‘waviness’ at a scale of mm providing the topography of the surface, and the small-scale roughness at a sub-millimetre scale.

At the scale of the experimental investigation, the flow through the fracture is expected to be controlled by the small-scale roughness of the fracture surface and the mismatch of the upper and lower surfaces. The larger-scale ‘waviness’ is not so relevant to the experimental data where the sample is of the order of cm long.

The fracture scan data are determined as x, y, z data; therefore, it is necessary to remove the influence of the larger-scale waviness to be able to assess the characteristics of the smaller-scale roughness. To do this, a low-resolution asperity reference surface (LRARS) was calculated by generating a linearly interpolated grid at a significantly coarser resolution than the detailed surface roughness. This grid, however, had a much higher resolution than the ‘waviness’. From the LRARS, a high-resolution asperity reference surface (HRARS) was generated at the resolution of the experimental data, the information from the LRARS being used to predict the surface profile of the HRARS. The HRARS was then used as a reference surface to evaluate the aperture profile and to determine the statistical

distribution of the small-scale asperity variation. These surface asperity data are illustrated in Fig. 13.

Fig. 13

High-resolution asperity surface distribution, and two statistically identical generated profiles fitting the data, where the mean value is 0.45 mm and the standard deviation is 0.025 mm

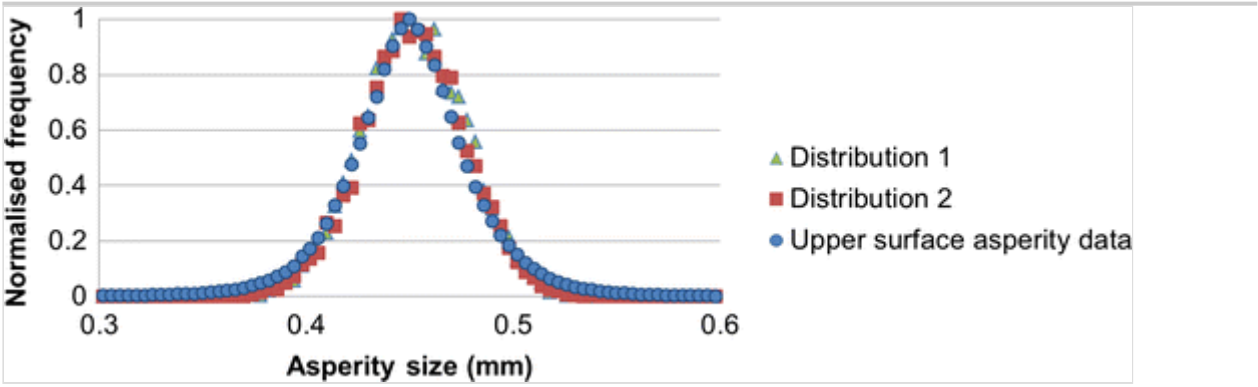

To generate the aperture data from the asperity data, two normal distributions are fitted to the asperity data (see Fig. 13, distribution fit 1 and 2), mathematically described by a normal distribution as:

$$X_1 = N\left(\mu, \sigma^2\right) \qquad 12$$
$$X_2 = N\left(\mu, \sigma^2\right)$$

The normal distributions are then fitted together as if each represented one surface of the fracture. The aperture is then evaluated as:

$$e = e_0 + m\left(X_1 - X_2\right) \qquad 13$$

where e_0 can be considered to be the average fracture aperture and m is the mismatch parameter between the two surfaces. The effects of the parameters e_0 and m on the simulated aperture distribution are illustrated in Fig. 14.

Fig. 14

Combination of two statistical distributions of the asperities on the fracture surface to create an aperture distribution accounting for mismatch of the surface profiles (see Eq. 13)

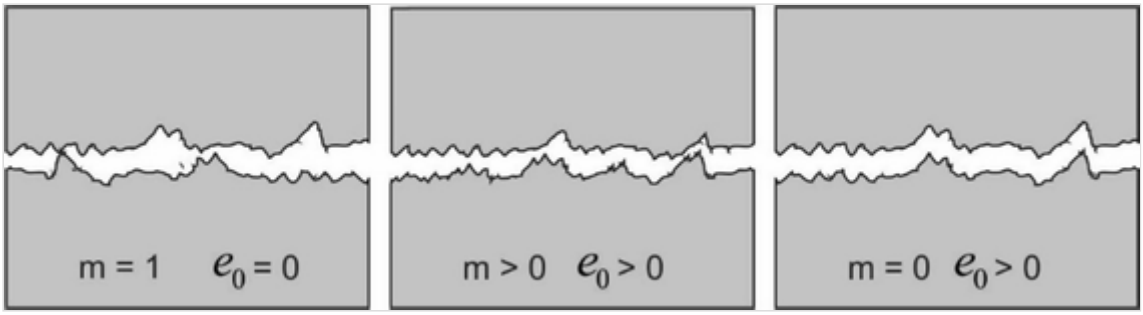

The aperture data were interpreted for the novaculite sample using Eq. (13), e_0 = 17 μm and m = 0.3. The resulting aperture distribution is illustrated in Fig. 15; the minimum aperture allowed in the simulations was 4×10^{-7} m.

Fig. 15

Aperture distribution predicted from the statistical distribution of the asperity data, e_0 = 0.017 mm, m = 0.3 (see Eq. 13)

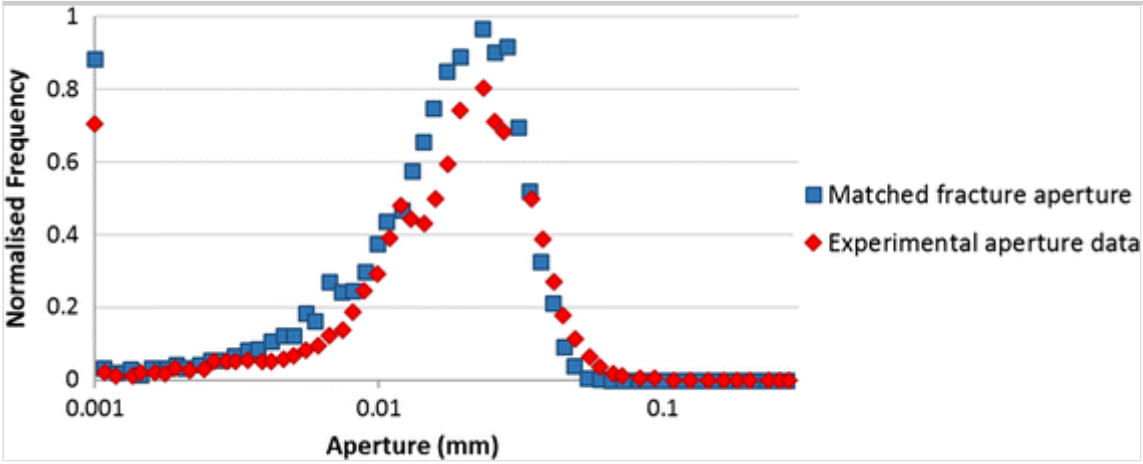

Various numerical techniques were adopted to allow the representation of rapid mechanical and chemical processes at small scales on relatively coarse grids to generate the fracture closure and then opening seen in the experimental data. These included the use of streamline dissolution to create the channelisation effects seen in the high-temperature novaculite data, i.e. the approach includes a detailed representation of localised aperture changes. Full information on the approach adopted is presented in Bond et al. (2015b) and McDermott et al. (2015)—for brevity, the details are not repeated here further. The technique has been extended to consider a more complete elastic response and nonlinear flows (McCraw et al. 2015).

In constructing their model, NRC noted that in the Yasuhara et al. (2011) mass balance formulation, the three processes of pressure dissolution at contacting area, diffusion in water film at areas of asperity contact, and precipitation or free face dissolution at the pore space walls are coupled to define the mass transport

through the system and the reduction of fracture aperture. Following this conceptual model, a revised mass balance equation was derived in Cao (2015) which contains extra terms that account for the volumetric changes of the interface region and the pore region. Without including these volumetric changes, the aperture reduction is overestimated; the mass flux from pressure dissolution and diffusion are not balanced, and Yasuhara chose to use mass flux from diffusion to estimate the aperture reduction. In the Cao's (2015) numerical simulation, the pressure dissolution mass flux is balanced with the diffusion mass flux (Eq. 11). Figure 16 illustrates the difference in the two mass balance approaches using otherwise identical inputs (see Cao 2015). It is noted that the numerical methods adopted by the other teams implicitly include this effect, but the behaviour had not been addressed in the earlier work of Yasuhara et al. (2006).

Fig. 16

Aperture reduction using Yasuhara et al. (2004) approach (*blue*, *solid line*), and the re-derived mass balance equations from Cao (2015) (*red*, *dashed line*). Neglecting the change in volume terms leads to overestimates of the mass flux removed, and consequently overestimates of the aperture reduction. The initial aperture was chosen at 12.5 (μm) when the initial contact ratio is 0.01

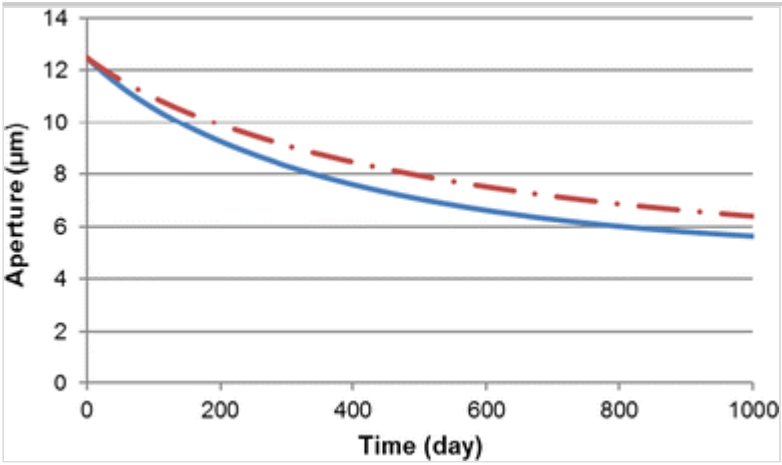

Calibration and model results

The results from each of the teams are presented in Figs. 17 and 18. All teams were able to produce a good calibration to the isothermal part of the experiment with a single consistent set of parameters. The major deviations from the experiment in most models arose around the time of the flow shutdown where the experiment shows an increase in effective hydraulic aperture, followed by a decrease along the same trend. Some speculations among the researchers suggest that this increase might have been caused by the relative fracture surface alignment changing slightly in the loss of confinement, but because it is not entirely clear what happened, it was considered unrealistic to expect the models to

be able to reproduce this feature. Further experiments using the same protocol would help address this uncertainty.

Fig. 17

Comparison of modelled versus observed hydraulic aperture (interpreted using the cubic law from the measured pressure differential as per Yasuhara et al. 2006)

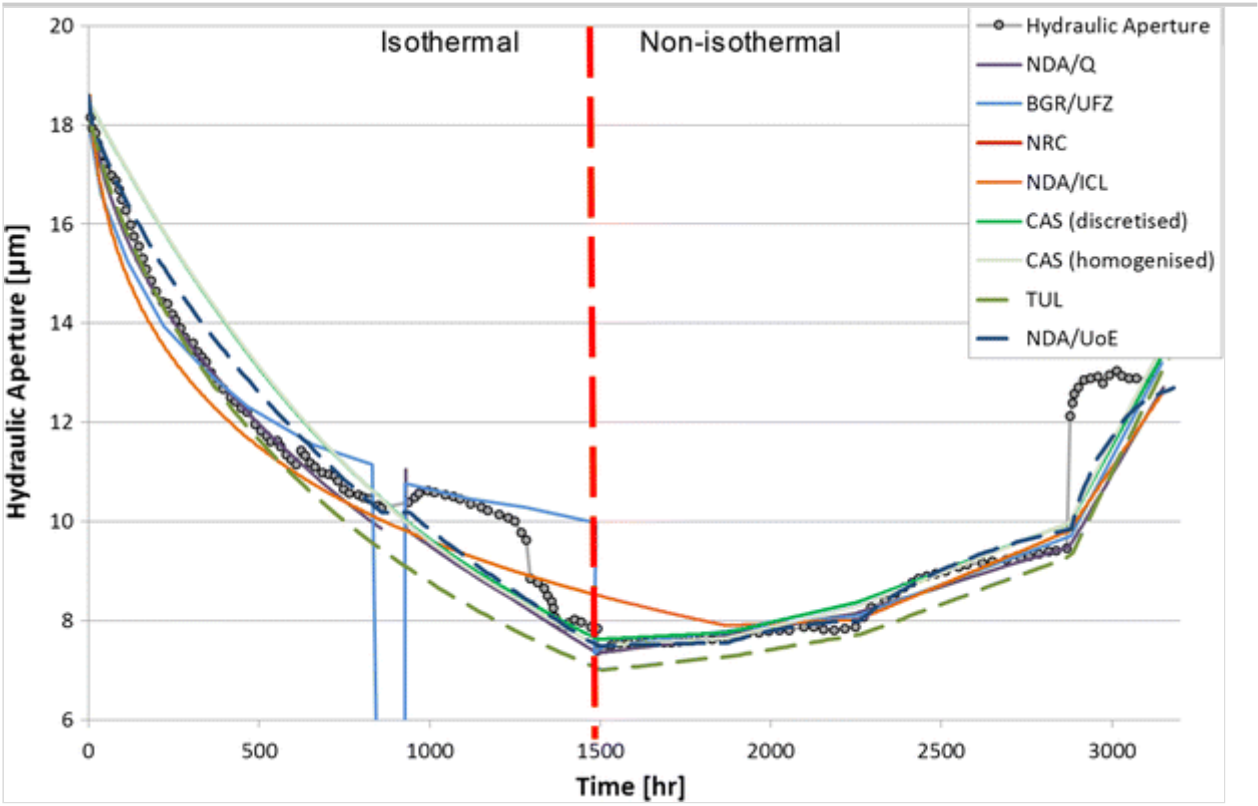

Fig. 18

Comparison of modelled versus observed Si concentration in the effluent (ppm)

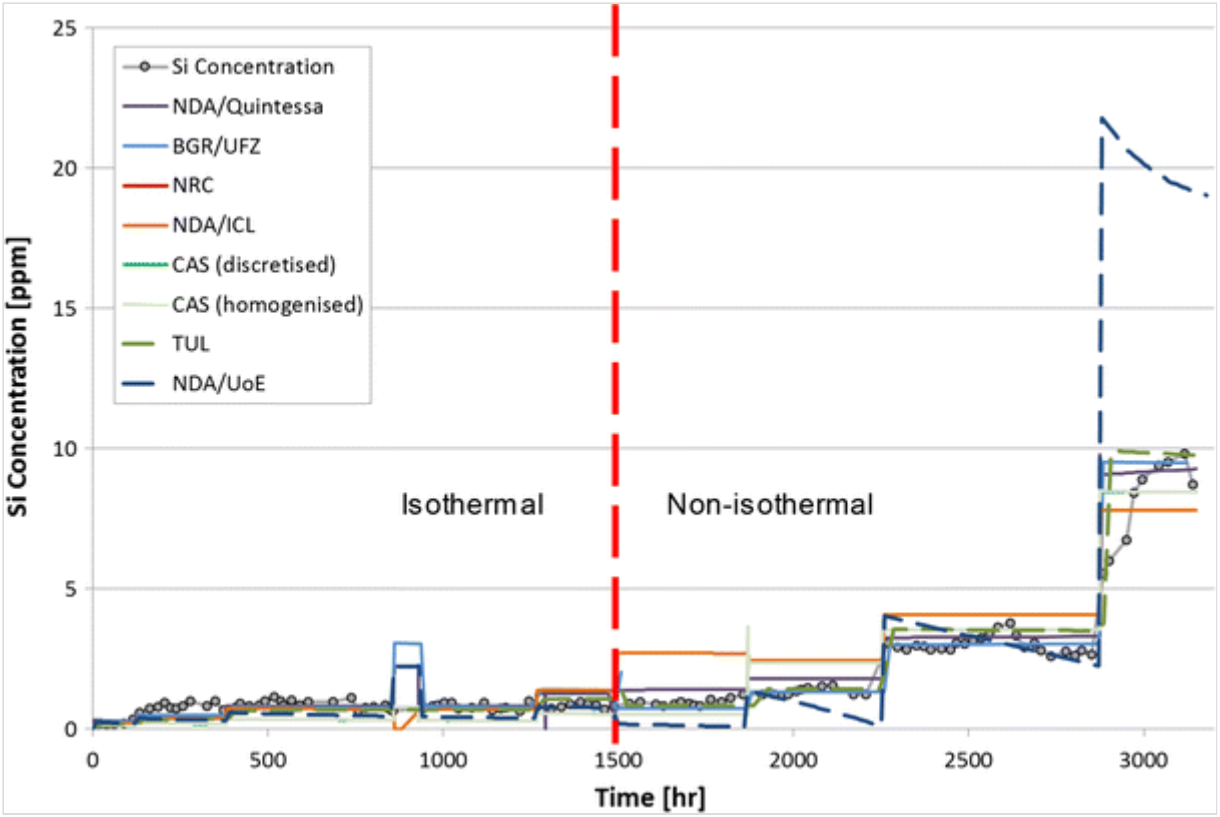

The parameterisation during this initial phase is consistent among the teams. All models which used the pressure solution model required that the effective rate term for the pressure solution (k^+) be scaled up from the reference values (e.g. Rimstidt 1997) by approximately 5 orders of magnitude in order to obtain both the aperture closure and silicon concentrations at the same magnitude as the observations. Such exaggeration of the expected physical parameters implies that the treatment of the parameterisation of the contact points is incorrect or the basic process model is in error. Even considering the uncertainty of the precise form of the SiO_2 mineral, which might give rise to a factor of 10 difference in solubilities and dissolution rates at most (Palandri and Kharaka 2004; Alexander et al. 1954; Gunnarson and Arnórsson 2000), such large calibration factors are hard to justify physically. Some teams (e.g. UoE, Q) also scaled up the free face dissolution by similar magnitudes allowing the pressure solution parameterisation to be adjusted and a better fit obtained. α and β_c values varied among calibrations depending on the details of the free dissolution model used, but α values typically were between 0.5 and 1 with β_c values zero (no critical stress limitation) to unity. This illustrates that the details of the assumptions regarding the ‘aperture’ model can have large impacts on the physical process parameterisation, but also illustrate that a range of acceptable calibrations are possible. Note that solute calculations are also made by the NRC team (Gwo et al. 2015), but these calculations were made with a sufficiently different end-point and as such did not use any rate or area enhancement terms as adopted by all the other teams. Consistent with the results

of other teams (BGR/UFZ, Q, UoE, ICL), the calculated concentrations are several orders of magnitude less than those observed.

For those teams who also represented the closure using stress corrosion, a different, but equally problematic parameterisation issue was found. While the closure of the aperture could be modelled using stress corrosion with reasonable and consistent values with previous publications (e.g. Yasuhara and Elsworth 2008), in order to reproduce the observed silicon concentrations in the effluent, the dissolution process had to be increased by again scaling the rate (which can be conceptualised as being the kinetic term or the effective reactive area) by the order of 10^5. Using such a parameterisation fitted the data well, but again suffers from the apparently artificial inflation of physically constrained parameters.

Conceptually, the increase in area can be attributed to the high degree of roughness of the fracture surface at small scales, but no analysis has yet been performed to justify such an effective area at the macro-scale is reflected by processes at the micro-scale, and so this remains speculation. However, it should also be noted that compared to pressure solution, stress corrosion as a process on fracture surfaces is not a well-studied subject. In particular, it is not clear how the stress corrosion process affects dissolution, and hence, a certain degree of caution should be applied to the use of the stress corrosion process.

The results in the isothermal period, and the consistency among the models, suggest that all three processes (pressure solution, stress corrosion and free face dissolution) might be operating, but distinguishing between the processes, especially when considering the large scaling factors that need to be applied, is difficult with the available data. In discussions between the teams, it became apparent that differences between the models during the isothermal period reflect more the calibration choices made by the teams in fitting the aperture data, rather than fundamental differences between the models.

In the non-isothermal part of the model, again the modelling results, in general, reflect the experimental results. However, in order to get the good fits shown by the Q, UoE and ICL models, some additional adjustments of parameters were needed as the temperatures change. Two additional calibrations were used. Firstly, the critical stress in the pressure solution or stress corrosion models had to be calibrated such that after 1494 h, hydraulic aperture reduction ceased (ICL, Q), or arbitrarily turned off these processes (UoE, BGR/UFZ) so that only dissolution dominates after 1494 h. The ICL results in particular show this behaviour as an emergent feature of the system (hence, the increase in aperture occurring later than the experiment), while the UoE and BGR/UFZ modelling imposed the shutdown in pressure solution in order to obtain a better fit. Indeed, for the BGR/UFZ model

the closure and opening parts of the experiment are treated as almost entirely different models with the hydraulic aperture not being continuous across the first temperature change.

~~Secondly, an additional scaling of the effective area associated with the dissolution process had to be applied and that decreased with temperature~~Secondly, an additional scaling of the effective area associated with the dissolution process which decreased with temperature, had to be applied. The scalings given in the BGR/UFZ, ICL and Q models are shown in Fig. 19. The comparison between the different modelling approaches is extremely strong for the Q and ICL results (about 3 orders of magnitude between 20 and 120 °C), suggesting that such scaling is physical, and not a result of modelling assumptions, although ICL found it necessary to enhance pressure solution more than free face dissolution to get an optimised fit. However, the BGR/UFZ model has a smaller difference (approximately 2 orders of magnitude between 20 and 120 °C) illustrating that while the basic requisite is the same between models, the magnitude of this additional factor is in part influenced by the details of the calibration and model setup. In addition to reducing the Yasuhara et al. (2004) critical stress parameter by a factor of 10, CAS made adjustments to both the rate of pressure solution and free face dissolution, but using discontinuities with time in the experiment rather than temperature as the primary variable (although clearly some of the intervals do correspond with temperature changes). The scaling factors are given in Table 1 and show the same general pattern as the other teams; the need to reduce the effectiveness of pressure solution (which in the case of UoE and BGR/UFZ is disabled completely at later times) and free face dissolution as temperatures rise and the experiment progresses.

Fig. 19

Calibrated reaction rate factors with temperature used by BGR/UFZ, ICL and Q. Note that ICL scale pressure solution and free face dissolution (F.F. Diss.) separately, while Q and BGR/UFZ apply the same rate enhancement to both processes

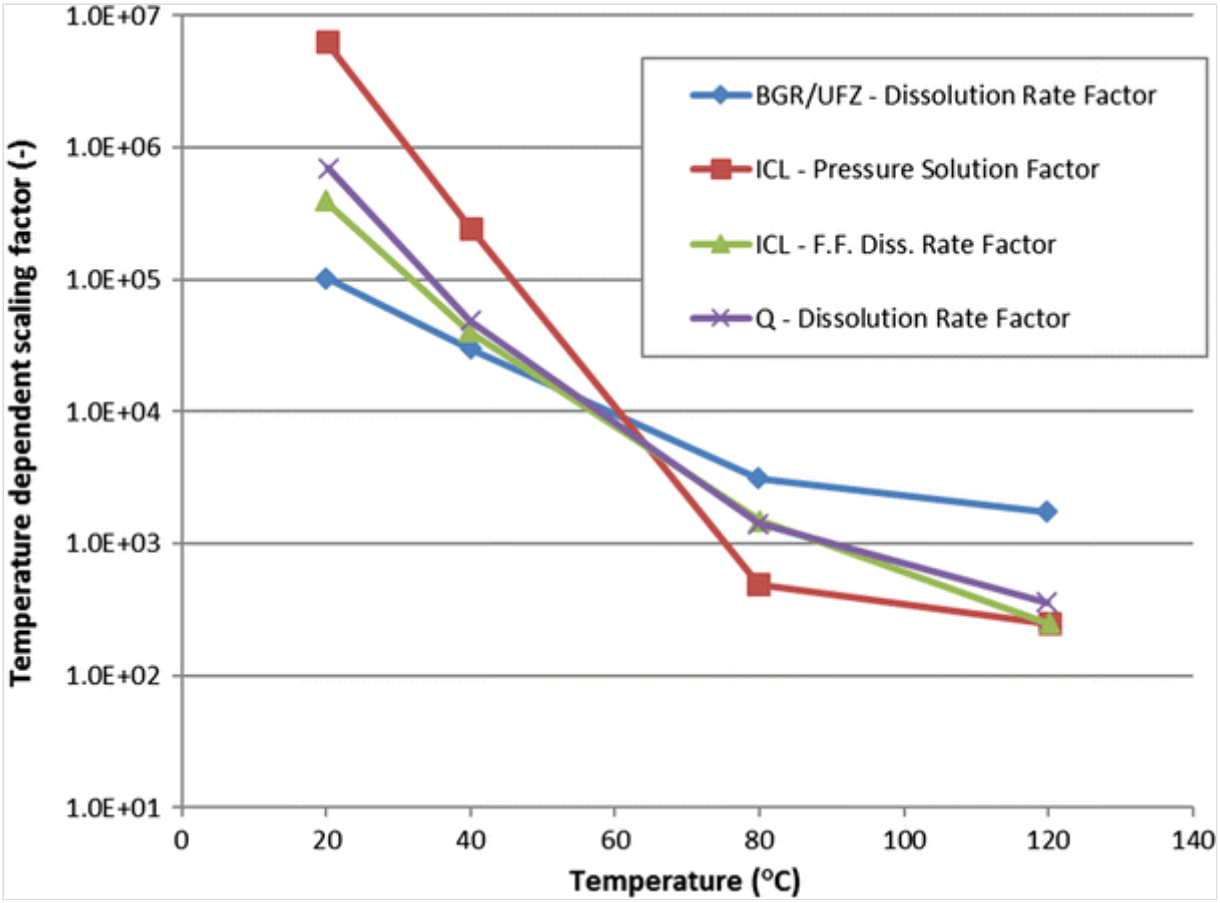

Table 1

Calibration scaling factors for the pressure solution and free face dissolution kinetic rates used by CAS

Time (h)	0–1292	1292–1869	1869–2255	2255–2875	2875–3150
CAS scaling factor on pressure solution (k_+)	$\times 10^6$	$\times 10^4$	$\times 10^4$	$\times 500$	$\times 200$
CAS scaling factor on free surface dissolution (k)	$\times 10^4$	$\times 10^4$	$\times 10^4$	$\times 500$	$\times 200$

AQ8

Thus, at high temperatures the net parameterisation of the dissolution rate is more consistent with a plane surface approximation to the fracture surface. One possible hypothesis is that increasing the temperature increases the Si diffusivity in the fluid. Increased diffusivity lessens the effect of differences in the thickness of any potential boundary layers at the micro-scale, which in turn might act to smooth some of the effect of roughness of the fracture surface at very small scales. The justification for reducing the pressure solution rate in a similar manner is less well-defined, however.

One further point can be obtained from comparing the Q, ICL, BGR/UFZ and UoE results. The UoE and BGR/UFZ and CAS discretised models have particular approaches for representing channelisation which causes an asymptotic change in effluent concentrations after each of the temperature changes. In contrast, the homogenised models of Q and CAS (which cannot represent channelisation in the current formulation) and the discretised model of ICL do not show this behaviour. The reason why the discretised model of ICL does not show this behaviour is not immediately clear, given that the UoE, CAS and BGR/UFZ models do. However, when considering the information supplied by the teams, it is likely to be because of modelling decisions relating to upwinding of flow velocities and associated contaminant transport to reflect sub-grid-scale effects. It seems likely that the UoE and BGR/UFZ models enhance this effect more than the ICL approach, giving rise to the different effluent behaviour. Including the net effect of this channelisation in the models, if indeed this is the cause of the concentration asymptotes, using some forms of upscaled process model would seem to be a necessary step to represent all features of the experimental result.

On the basis of this result, Fig. 20 is proposed by UoE as a means of illustrating the relative importance of different processes where it is assumed that pressure solution is the dominant aperture closure mechanism. A full discussion of their approach is given in McDermott et al. (2015).

Fig. 20

Suggestion of relative process importance in a pressure-solution-dominated system by UoE (reproduced from McDermott et al. 2015)

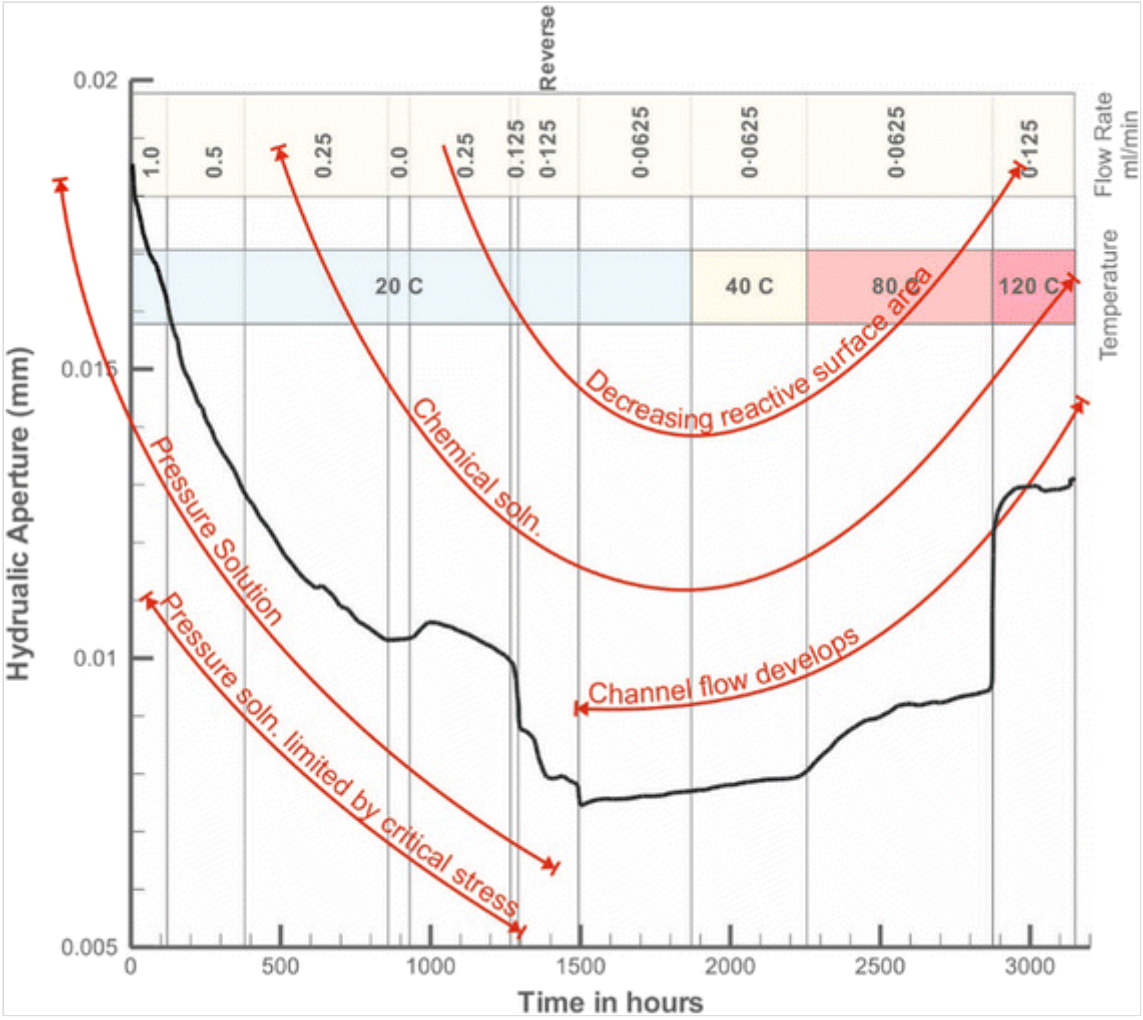

Aperture representation issues

When considering the aperture distribution input to the homogenised and discretised approaches, it was recognised that there was a potential sensitivity to the details of the fracture surface topography data. The laser profilometer data were captured over the area of 89 mm by 45.95 mm on a 50-μm resolution grid (i.e. most, but not all of the surface) and have a stated precision of 0.5 μm plus 5 μm per 2 °C temperature variation (hence, +10 μm over the duration of the measurement) vertically and 15 μm in the fracture plane. It is also noted in Yasuhara et al. (2006) that there is a systematic relative tilt in the topography data that required correction.

Given this observed bias, it was decided to analyse the fracture topography data to consider the possibilities and consequences of further bias in the data including:

- Tilt (systematic relative rotation of surfaces in the plane of the fracture)
- Rotation (systematic relative rotation of surfaces out of the plane of the fracture)
- Offset (misalignment of the surfaces in the plane of the fracture).

The possibility of offset over small distances may also come about due through the process of initial separation and reassembly of the fracture during the measurement and experimental construction, despite the extreme care taken by the experimentalists.

An automated brute-force search was conducted by offsetting one surface relative to the other surface by integer measurement point in the fracture plane, examining the apparent surface difference variance and systematic skews across the profiles in each case. One ‘fit’, moving the upper surface one measurement grid cell (50 μm) in the negative x direction, was found to be objectively better than all others, reducing the maximum and minimum difference between surfaces, reducing the variance along profiles across the surface and maximising the visibility of skews in the data. The apparent skew was a simple bilinear feature consistent with the fracture sample not being completely relatively horizontal when measured. The skew correction applied to the top surface is as follows:

$$\Delta z = 1.00265 \times 10^{-4} x - 3.5499 \times 10^{-5} y \qquad 14$$

where x, y are the surface coordinates (mm) and Δz is the change in topography to the top surface (mm).

The comparison of the uncorrected offset and offset data with bilinear correction is shown in Fig. 22. In addition to reducing the range of differences between the surfaces, the application of an offset makes the zero point (no offset between the surfaces has been made in this case; hence, a zero value indicates a perfect fit between surfaces) close to the centre of the range of data allowing the skew along the long axis of the fracture to be visible as well as an apparent radial pattern. Removing the skew (Fig. 21) again allows the radial pattern to be visible. Whether this radial pattern is a function of the creation of the fracture, or a reflection of another, smaller-scale rotational mismatch between the surfaces is open to interpretation. Making these small changes at the scale of the stated errors of the measurement clearly improves the ‘fit’ of the two fracture surfaces.

Fig. 21

Plot of the difference between the *top* and *bottom* surfaces (zero datum) with no correction (*top*, **a**), offset applied (*middle*, **b**) and offset with skew correction (*bottom*, **c**). Difference units are in mm

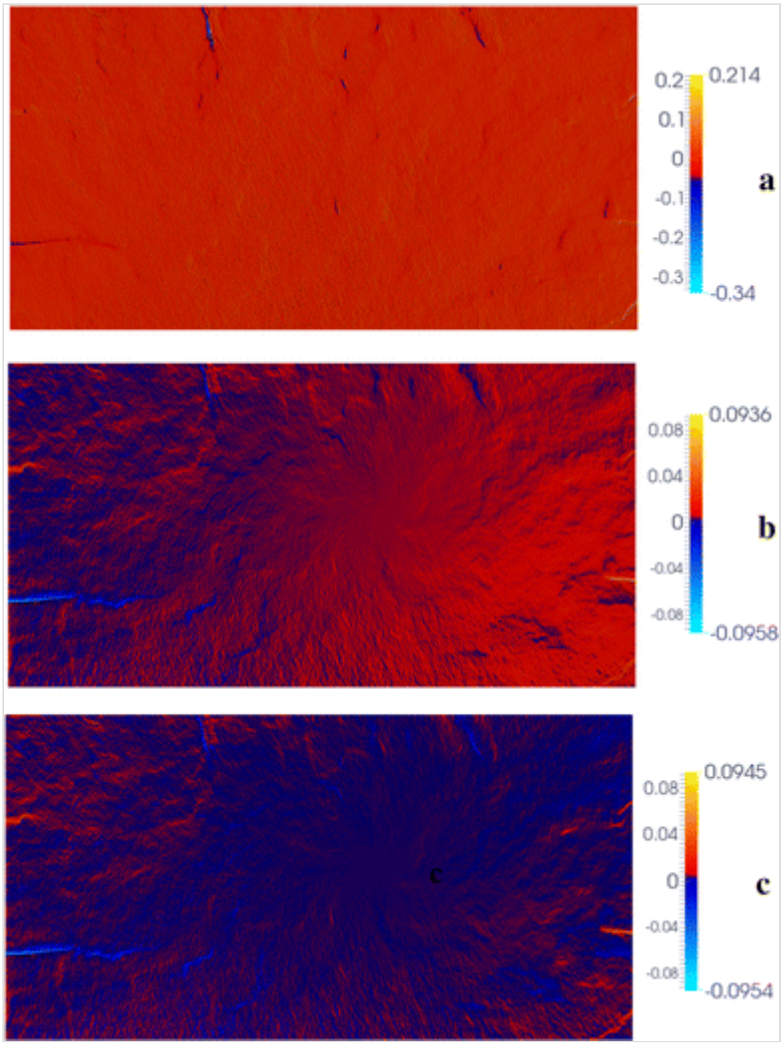

When comparing the effective permeability distributions of the reference data with the corrected data set (having applied an offset between the surfaces to obtain the same net permeability) using the pressure solution, discretised approach of UoE, one can immediately see the corrected data set gives a tighter permeability distribution (Fig. 22). While this different permeability distribution changed the results significantly, it was found to be possible to recalibrate the model reflecting the difference in contact ratio, reducing the effective rate of pressure dissolution by approximately an order of magnitude (noting this is still small in comparison with the other empirical scaling factors applied to the pressure solution model).

Fig. 22

Normalised frequency distribution of intrinsic permeability for the reference data set and the corrected data set as corrected to the required initial fracture permeability using the UoE model

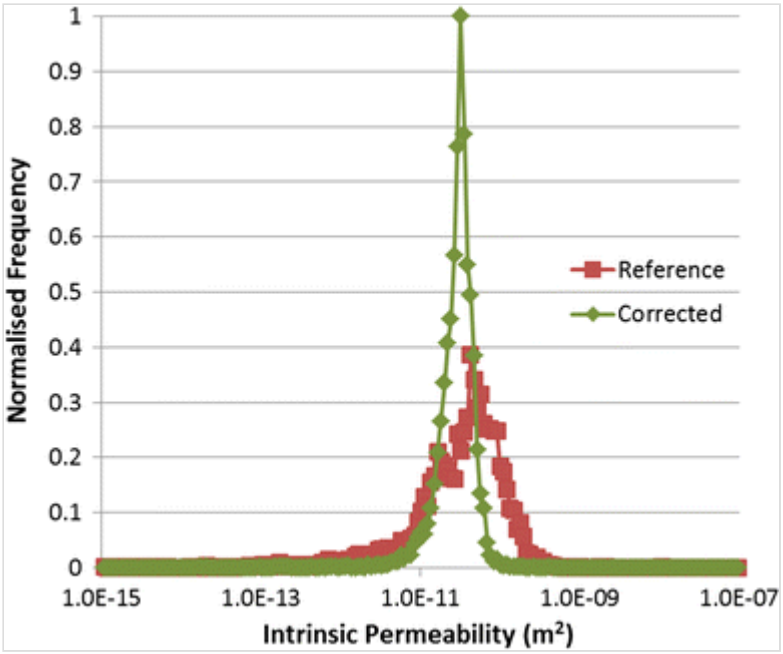

Following this result, it was questioned how useful the profilometer data are in directly deriving the aperture distributions. This result emphasises the need to use measurements of fracture topography in place of derived aperture when calculating fracture characteristics of statistical, multi-scale representations of the fracture that are based on the experimental data. The discrete data do, however, serve to allow the ongoing investigation of micro-scale processes such as the development of possible channel flow.

Inclusion of rock matrix diffusion

One suggestion for the physical process behind the need to artificially enhance dissolution rates in order to fit the observed effluent Si concentrations was to invoke rock matrix diffusion (RMD—Neretnieks 2014). Essentially, this process adds to the area over which dissolution of quartz can occur, but limits the transport of the dissolved Si to the fracture by a diffusive process. Neretnieks (2014) concluded that RMD is likely to be a significant contributor to Si concentrations in the effluent especially at elevated temperatures.

To cross-check these calculations, the Q homogenised model was adjusted to include a RMD process and parameterised in a similar manner to the Neretnieks (2014) calculations (Fig. 23; Table 2; Bond et al. 2015b). Using this model, the homogenised calculations were re-run with the free face dissolution scaling coefficient reduced from 7×10^5 to 1. The model assumes a fully connected porosity which is water-saturated and has a large specific area for fluid–mineral interactions. It should be noted that there is no direct evidence for the porosity structure or water content of the novaculite, so these assumptions are quite open to challenge; however, the values have been selected to be conservative in the sense that RMD will be tend to be overestimated.

Fig. 23

Conceptual model for pressure solution, effluent advection and rock matrix diffusion (from Neretnieks 2014). The symbols starting *c* denote different concentrations, A_s and A_{md} are the areas associated with pressure solution and matrix diffusion, respectively, *b* is the aperture, and $\sigma_{e,s}$ is the pressure solution stress

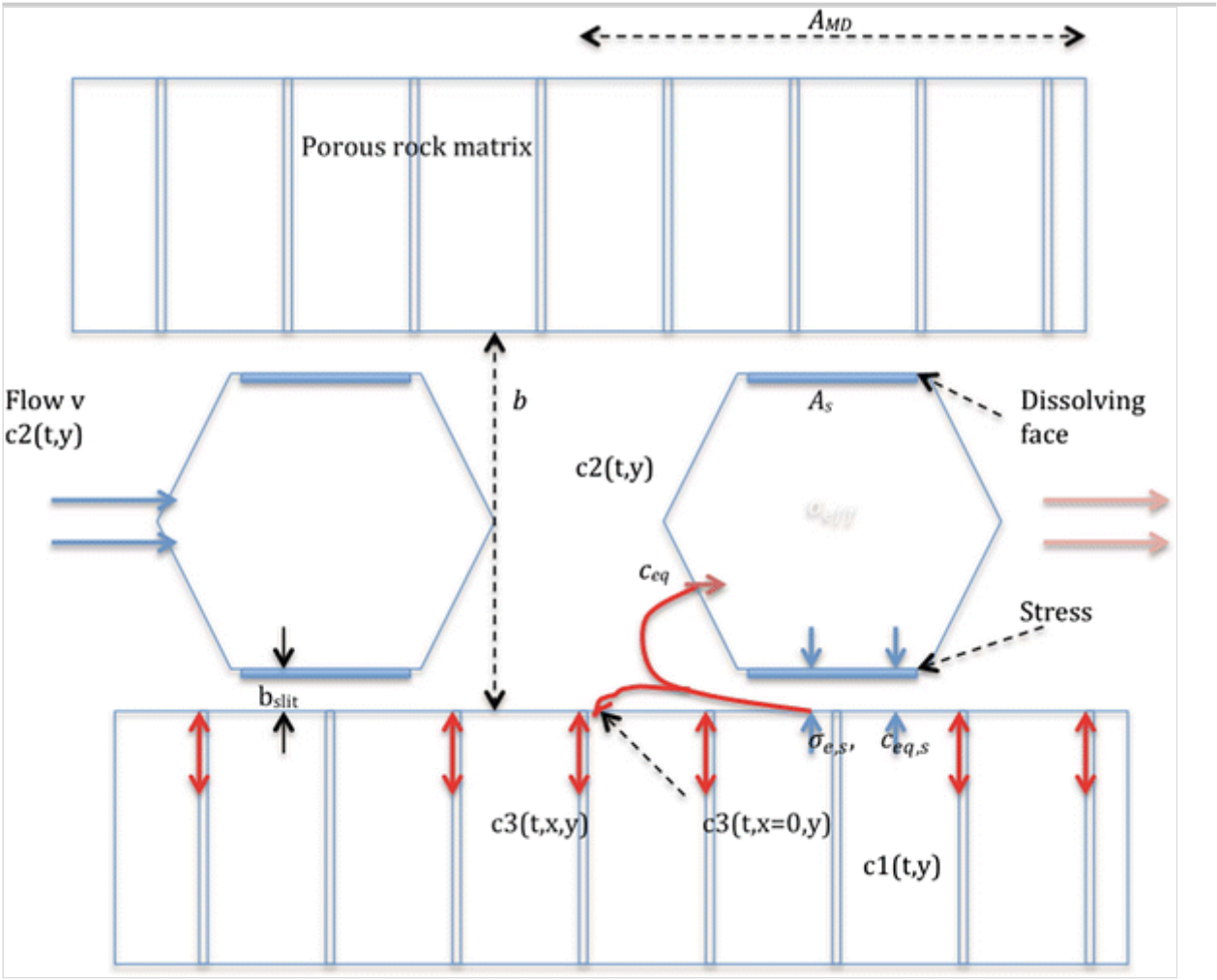

Table 2

Rock matrix diffusion parameters for the Q homogenised model (all values assumed)

Parameter	Description	Value	Unit
θ	Novaculite porosity	0.01	–
A_{rock}	Rock internal surface area (based on 1 μm dia. spherical grains)	2.26	m^2/g
τ	Tortuosity	0.33	–
D_{pore}	Pore-water Si diffusion coefficient	1×10^{-9}	m^2/s

The results were found to be very sensitive to grid refinement away from the fracture (Fig. 24), but grid-converged results were obtained which showed that RMD, as parameterised, could achieve the dissolved Si concentrations seen at elevated temperatures (Fig. 25). However, at the initial temperature, the dissolved concentrations are far too low in comparison with the data. Some speculation was entered into that the RMD might be occurring as described, with colloidal Si making up the observed effluent at lower temperatures; however, there was no evidence to justify this hypothesis.

Fig. 24

Illustration of rock matrix attached to fracture for the Q homogenised model (*blue arrow* indicates fluid flow; *green arrows* indicate interaction of the fracture fluid and the rock by surface processes and matrix diffusion)

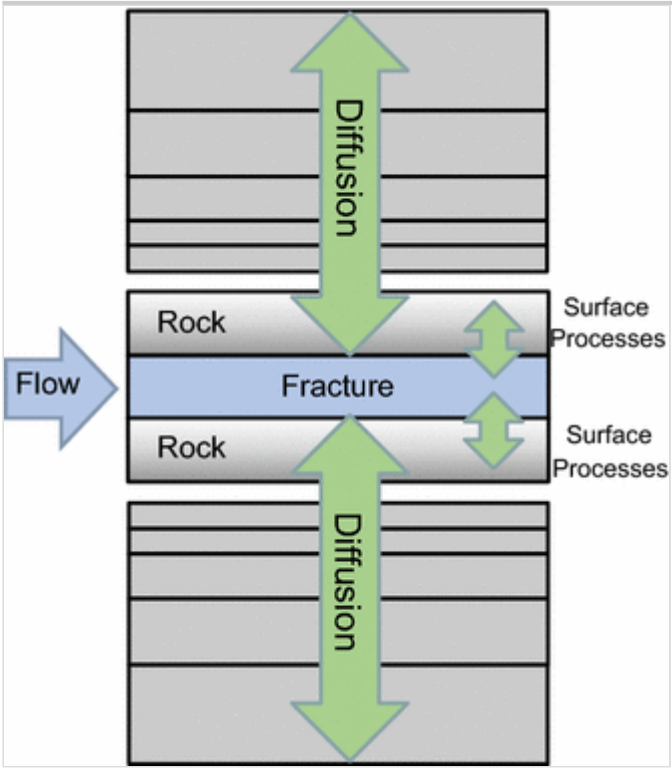

Fig. 25

Si concentration comparison of the experiment and coarse (5 cells, 2-mm initial cell) + fine (50 cells, 0.02-mm initial cell) rock matrix diffusion models applied to novaculite fracture flow with no roughness factors

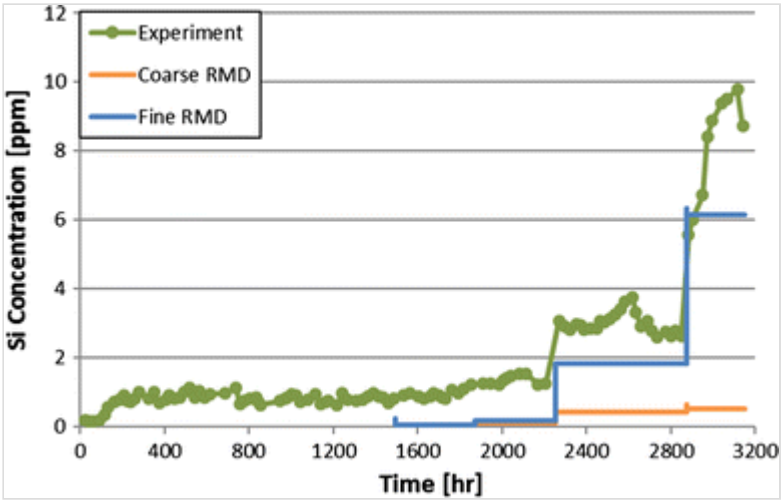

The calculations of Neretnieks (2014) and the modified Q model show that RMD has the potential to provide the observed high concentrations of Si at elevated temperatures; however, this requires a water-saturated, well-connected pore structure, and it is unclear whether these conditions are found in the tested novaculite sample. Overall, there is the potential for rock matrix diffusion to contribute to higher solute effluent concentrations by effectively providing a larger surface area over which chemical processes can act, especially over longer timescales, but this process cannot explain all the observations.

Initial comparison with other experimental data

NRC and TUL performed an initial application of their homogenised models to a natural fracture in an almost identical Arkansas novaculite as used in the Yasuhara et al. (2006) experiment (Gwo et al. 2015). This earlier work by Polak et al. (2003) also considered a vertical column experiment under variable differential fluid pressures and temperatures. The work suggested that while the calibration of critical parameters relating to the aperture and asperity distribution needed to be changed between analyses, the basic framework appeared equally applicable to both natural and artificial fractures. However, such comparisons are at a very preliminary stage and will be a major component of future work and so are not discussed here further.

Discussion

The multi-team approach has shown that a range of models can be applied to the novaculite data and obtain a fit with both the aperture closure and silicon concentration discharge. However, in order to obtain these fits, use of various (often very large and context-dependent) ‘calibration’ factors tends to imply that key aspects of the physical model have not been well captured. These changes in calibration properties can have plausible physical explanations, but there is still uncertainty in making predictions based on available physical models under

dynamic flow conditions and time-dependent thermal loads. This uncertainty is compounded by a general inability to distinguish between the pressure solution and stress corrosion closure models on the basis of the available data. Furthermore, the direct use of the fracture topography surfaces to construct aperture distributions, while tempting, appears to give the potential for skewing results and a high degree of sensitivity on the macroscopic model calibration.

However, there appears to be considerable promise in the use of statistical representations of the fracture surface that allow different processes in the fluid and the fracture surface to interact at the 'correct' spatial scale. It is hoped that such an approach will provide a mechanism to better understand and predict the variation of macroscopic (single-fracture) 'calibration' parameters to relatively simple process models and, hence, permit THMC analysis of this type to move beyond the single-fracture scale.

Acknowledgements

The authors appreciate and thank the funding organisations for their financial and technical support of the DECOVALEX project work described in this paper. In part, this work was financially supported by National Natural Science Foundation of China (Nos. 51322906, 41272349). The statements made in the paper are, however, solely those of the authors and do not necessarily reflect those of the funding organisation(s).

Appendix: Codes and modelling approaches

See Table 3.

Table 3

Codes and general modelling approaches used by the teams in this study

Team	Code(s)	Code references	Treatment of aperture data	Mathematical model
BGR/UFZ	OpenGeoSys	Kolditz et al. (2012)	Synthetic	N/A
CAS	EPCA	Feng et al. (2006), Pan et al. (2009, 2011), Pan and Feng (2013)	Discretised	2D aperture closure, transport, geochemistry
ICL	CSMP ++	Matthäi et al. (2005) and Paluszny et al. (2007)	Synthetic	2D elastic closure (REV model), flow, geochemistry
				1D transport

Team	Code(s)	Code references	Treatment of aperture data	Mathematical model
NRC	HBGC123D	Gwo et al. (2001)	Homogenised	0D aperture closure, flow, transport, geochemistry
	Mass balance approach			
Q	QPAC	Bond et al. (2012) and Quintessa (2013)	Homogenised	0D aperture closure, flow, transport, geochemistry
TUL	X2t (part of GWB)	Bethke and Yeakel (2013)	Discretised	2D aperture closure, flow, transport, geochemistry
UoE	OpenGeoSys	Bond et al. (2012) and Quintessa (2013)	Synthetic	2D aperture closure and flow
				2D semi-analytical transport
				2D inverse geochemistry

References

Alexander GB, Heston WM, Iler RK (1954) The solubility of amorphous silica in water. J Phys Chem 58:453

Atkinson BK (1987) Fracture mechanics of rock. Academic Press, London

Berkowitz B (2002) Characterizing flow and transport in fractured geological media: a review. Adv Water Resour 25(8):861–884

Bethke CM, Yeakel S (2013) Reactive transport modeling guide. Aqueous Solutions, LLC, Champaign. http://gwb.com/pdf/GWB9/GWBtransport.pdf

Bond A (2016) Task C1 Final Report. KTH Report ISBN 978-91-7595-829-3(06), ISSN 1650-86-10

Bond AE, Benbow S, Wilson J, McDermott C, English M (2012) Coupled hydro–mechanical–chemical process modelling argillaceous formations for DECOVALEX-2011. Mineral Mag 76(8):3131–3143

Bond A, Thatcher K, Chittenden N, McDermott C, Fraser-Harris A (2015a) RWM Coupled Processes Project: First Annual Report for RWM participation in DECOVALEX-2015 Tasks A and C1. AMEC report 18040-TR-002 v2.0. RWM Peer Reviewed Technical Report. https://rwm.nda.gov.uk/publication/rwm-coupled-processes-project-first-annual-report-for-rwm-participation-in-decovalex-2015-tasks-a-and-c1/

Bond A, Thatcher K, Chittenden N, McDermott C, Fraser-Harris A (2015b) RWM Coupled Processes Project: Second Annual Report for RWM participation in DECOVALEX-2015 Tasks A and C1. AMEC report 18040-TR-003 v3.0. RWM Peer Reviewed Technical Report. https://rwm.nda.gov.uk/publication/rwm-coupled-processes-project-second-annual-report-for-rwm-participation-in-decovalex-2015-tasks-a-and-c1/

Bond AE, Brusky I, Cao T, Chittenden N, Fedors R, Feng X-T, Gwo J-P, Lang P, McDermott C, Neretnieks I, Pan PZ, Šembera J, Watanabe N, Zheng H (2016) Development of approaches for modelling coupled thermal–hydraulic–mechanical–chemical processes in single granite fracture experiments. http://www.decovalex.org/resources.html#special-issues

Brown SR, Scholz CH (1985) Closure of random elastic surfaces in contact. J Geophys Res 90(B7):5531

Cao T (2015) Mass balance equations for a single fracture, DECOVALEX-2015 Task C1. Intra-office Note to J. Rubenstone October 28, 2015, U.S. Nuclear Regulatory Commission. ADAMS ML15301A815. http://www.nrc.gov/reading-rm/adams.html

Chittenden N, McDermott CI, Bond AE, Wilson J, Norris S (2016) Evaluating the importance of different coupled thermal, hydraulic, mechanical and chemical process simulations during fluid flow experiments in fractured novaculite and fractured granite. http://www.decovalex.org/resources.html#special-issues

Dove PM, Crerar DA (1990) Kinetics of quartz dissolution in electrolyte solutions using a hydrothermal mixed flow reactor. Geochim Cosmochim Acta 54:955–969

Eyring H (1935) The activated complex in chemical reactions. J Chem Phys 3(2):107–115

Feng XT, Pan PZ, Zhou H (2006) Simulation of the rock microfracturing process under uniaxial compression using an elasto-plastic cellular automaton. Int J Rock Mech Min Sci 43(7):1091–1108

AQ9

Fetter CW (1994) Applied hydrogeology, 3rd edn. Prentice Hall, Englewood Cliffs

Gunnarson I, Arnórsson S (2000) Amorphous silica solubility and the thermo dynamic properties of H_4SiO_4 in the range of 0° to 350 °C at Psat. Geochim Cosmochim Acta 64:2295–2307

Gwo JP, D'Azevedo EF, Frenzel H, Mayes M, Yeh G-T, Jardine PM, Salvage KM, Hoffman FM (2001) HBGC123D: a high-performance computer model of coupled hydrogeological and biogeochemical processes. Comput Geosci 27:1231–1242

Gwo J, Cao T, Fedors R, Rubenstone J (2015) Modeling the coupled hydrogeochemical and mechanical behavior of a single artificial fracture in novaculite rock. In: Proceedings paper for the international high-level radioactive waste management conference. American Nuclear Society, La Grange Park

Johnson JW, Oeklers EH, Helgeson H (1992) SUPCRT92: a software package for calculating the standard molal thermodynamic properties of minerals, gases, aqueous species, and reactions for 1–5000 bar and 0–1000 °C. Comput Geosci 18:899–947

Kolditz O, Bauer S, Bilke L, Böttcher N, Delfs JO, Fischer T, Görke UJ, Kalbacher T, Kosakowski G, McDermott CI, Park CH, Radu F, Rink K, Shao H, Shao HB, Sun F, Sun YY, Singh AK, Taron J, Walther M, Wang W, Watanabe N, Wu N, Xie M, Xu W, Zehner B (2012) OpenGeoSys: an open-source initiative for numerical simulation of thermo–hydro–mechanical/chemical (THM/C) processes in porous media. Environ Earth Sci 67(2):589–599

Lang PS, Paluszny A, Zimmerman RW (2015) Hydraulic sealing due to pressure solution contact zone growth in siliciclastic rock fractures. J Geophys Res Solid Earth 120(6):4080–4101. doi:10.1002/2015JB011968

Matthäi SK, Mezentsev AA, Pain CC, Eaton MD (2005) A high-order TVD transport method for hybrid meshes on complex geometry. Int J Numer Methods Fluids 47:1181–1187

McCraw C, Edlmann K, Miocic J, Gilfillan S, Haszeldine S, McDermott C (2016) Experimental investigation and hybrid numerical analytical hydraulic mechanical simulation of supercritical CO_2 flowing through a natural fracture in caprock. Int J Greenhouse Gas Control. Volume 48, Part 1, May 2016, Pages 120–133. http://dx.doi.org/10.1016/j.ijggc.2016.01.002
AQ10

McDermott C, Bond A, Fraser-Harris A, Chittenden N, Thatcher K (2015) Application of hybrid numerical and analytical solutions for the simulation of coupled thermal hydraulic mechanical and chemical processes during fluid flow through a fractured rock. http://www.decovalex.org/resources.html#special-issues

Neretnieks I (2014) Stress-mediated closing of fractures—impact of matrix diffusion. J Geophys Res Solid Earth 119(5):4149–4163

Neuman SP (2005) Trends, prospects and challenges in quantifying flow and transport through fractured rocks. Hydrogeol J 13(1):124–147

Palandri JL, Kharaka YK (2004) A compilation of rate parameters of mineral-water interaction kinetics for application to geochemical modelling. US Geological Survey Open File Report 2004-1068. https://pubs.usgs.gov/of/2004/1068/pdf/OFR_2004_1068.pdf

Paluszny A, Matthäi SK, Hohmeyer M (2007) Hybrid finite element-finite volume discretization of complex geologic structures and a new simulation workflow demonstrated on fractured rocks. Geofluids 7(2):186–208

Pan PZ, Feng XT, Huang XH, Cui Q, Zhou H (2009) Coupled THM processes in EDZ of crystalline rocks using an elasto-plastic cellular automaton. Environ Geol 57(6):1299–1311

Pan P-Z, Feng X-T, Xu D-P, Shen L-F, Yang J-B (2011) Modelling fluid flow through a single fracture with different contacts using cellular automata. Comput Geotech 38(8):959–969

Pan P-Z, Feng X-T, Zheng H, Bond A (2016) An approach to simulate the THMC process in single novaculite fracture using EPCA. http://www.decovalex.org/resources.html#special-issues

Quintessa (2013) QPAC: Quintessa's General-Purpose Modelling Software. QRS-QPAC-11. www.quintessa.org/qpac

Rimstidt JD (1997) Quartz solubility at low temperatures. Geochim Cosmochim Acta 61:2553–2558

Schmittbuhl J, Schmitt F, Scholz C (1995) Scaling invariance of crack surfaces. J Geophys Res 100:5953–5973

Taron J, Elsworth D, Min KB (2009) Numerical simulation of thermal–hydrologic–mechanical–chemical processes in deformable, fractured porous media. Int J Rock Mech Min Sci 46(5):842–854

Tester JW, Worley WG, Robinson BA, Grigsby CO, Feerer JL (1994) Correlating quartz dissolution kinetics in pure water from 25 to 625 °C. Geochim Cosmochim Acta 58:2407–2420

Walsh J (1981) Effect of pore pressure and confining pressure on fracture permeability. Int J Rock Mech Min Sci Geomech 18(5):429–435

Watson C, Wilson J, Savage D, Benbow S, Norris S (2016) Modelling reactions between alkaline fluids and fractured rock: the Maqarin natural analogue. Appl Clay Sci 121–122:46–56

Yasuhara H, Elsworth D (2006) A numerical model simulating reactive transport and evolution of fracture permeability. Int J Numer Anal Methods Geomech 30(10):1039–1062

Yasuhara H, Elsworth D (2008) Compaction of a rock fracture moderated by competing roles of stress corrosion and pressure solution. Pure Appl Geophys 165:1289–1306

Yasuhara H, Elsworth D, Polak A (2004) Evolution of permeability in a natural fracture: significant role of pressure solution. J Geophys Res 109:B03204

Yasuhara H, Polak A, Mitani Y, Grader A, Halleck P, Elsworth D (2006) Evolution of fracture permeability through fluid–rock reaction under hydrothermal conditions. Earth Planet Sci Lett 244:186–200

Yasuhara H, Kinoshita N, Ohfuji H, Lee DS, Nakashima S, Kishida K (2011) Temporal alteration of fracture permeability in granite under hydrothermal conditions and its interpretation by coupled chemo-mechanical model. Appl Geochem 26:2074–2088

Zhang Y-J, Yan C-S, Xu G (2012) FEM analyses for T-H-M-M coupling processes in dual-porosity rock mass under stress corrosion and pressure solution. J Appl Math, Article ID 983718, 21 pages. doi:10.1155/2012/983718

Dove PM (1995) Geochemical controls on the kinetics of quartz fracture at subcritical tensile stresses. Journal of Geophysical Research: Solid Earth 100 (B11):22349-22359

Poon, C., Sayles, R., & T. Jones. 1992. Surface measurement and fractal characterization of naturally fractured rocks. Journal of Physics D: Applied 25:1269.

Zimmerman RW; Kumar S and GS Bodvarsson. 1991. Int. J. Rock Mech. Min. ScL & Geomech. dbstr. Vol. 28, No. 4. pp. 325-331. 1991

A. Polak, D. Elsworth, H. Yasuhara, A. S. Grader, P. M. Halleck, A. Polak, D. Elsworth, H. Yasuhara, A. S. Grader, P. M. Halleck, (2003) Permeability reduction of a natural fracture under net dissolution by hydrothermal fluids. Geophysical Research Letters 30 (20):2020

Pan P.Z., Feng X.T. (2013). Numerical study on coupled thermo-mechanical processes in Äspö Pillar Stability Experiment. Journal of Rock Mechanics and Geotechnical Engineering 5(2): 136-144.